

**Sea level-controlled sediment transport to the eastern Arabian Sea over the past 600 kyr: Clay minerals and Sr-Nd isotopic evidence from IODP Site U1457**

**Zhaojie Yu<sup>1,2\*</sup>, Christophe Colin<sup>2</sup>, Shiming Wan<sup>1,3</sup>, Rajeev Saraswat<sup>4</sup>, Lina Song<sup>5</sup>, Zhaokai Xu<sup>1,3</sup>, Peter Cliff<sup>6</sup>, Huayu Lu<sup>7</sup>, Mitchell Lyle<sup>8</sup>, Denise Kulhanek<sup>9</sup>, Annette Hahn<sup>10</sup>, Manish Tiwari<sup>11</sup>, Ravi Mishra<sup>11</sup>, Serge Miska<sup>2</sup>, Anil Kumar<sup>12</sup>**

- 1 Key Laboratory of Marine Geology and Environment, Institute of Oceanology, Chinese Academy of Sciences, Qingdao 266071, China
- 2 Laboratoire GEOsciences Paris-Sud (GEOPS), UMR 8148, CNRS-Université de Paris-Sud, Université Paris-Saclay, Bâtiment 504, 91405 Orsay Cedex, France
- 3 Laboratory for Marine Geology, Qingdao National Laboratory for Marine Science and Technology, Qingdao 266061, China
- 4 Micropaleontology Laboratory, Geological Oceanography Division, National Institute of Oceanography, Goa, India
- 5 Key Laboratory of Ocean Circulation and Waves, Institute of Oceanology, Chinese Academy of Sciences, Qingdao 266071, China
- 6 Department of Geology and Geophysics, E235 Howe-Russell-Kniffen Geoscience Complex, Louisiana State University, LA 70803, USA
- 7 School of Geographical and Oceanographical Sciences, Nanjing University, Nanjing 210023, China
- 8 College of Earth, Ocean and Atmospheric Sciences, Oregon State University, Corvallis OR 97331, USA
- 9 International Ocean Discovery Program, Texas A&M University, College Station TX 77845, USA
- 10 MARUM, University of Bremen, Bremen 28359, Germany
- 11 National Centre for Antarctic and Ocean Research (NCAOR), Goa 403804, India
- 12 Department of Science and Technology, Wadia Institute of Himalayan Geology, Utrakhnad 248001, India

\*Corresponding author: yuzhj1988@gmail.com, Tel.: +86 15698159660.

**Abstract**

Long marine sequences deposited in the Arabian Sea are suitable to study the orbital sensitivity of sediment dynamics from a source-to-sink perspective. The clay mineralogy and Sr-Nd isotopic compositions have been analyzed for the detrital fraction of sediments from IODP Site U1457 located in the Laxmi basin, eastern Arabian Sea to constrain the sediment sources and reconstruct a high-resolution record of sediment export to the Indus deep-sea fan over the past 600 kyr. The  $^{87}\text{Sr}/^{86}\text{Sr}$  ratio (varying from 0.7154 to 0.7255) and  $\epsilon\text{Nd}$  (varying from -12.9 to -9.5) imply a mixing of sediments derived from not only the Indus River but also the rivers draining the Deccan Traps. The variations in the smectite/(illite+chlorite) ratio combined with Sr-Nd isotopes permit the reconstruction of past changes in the relative proportions of sediments derived from the Indus River (mainly illite, chlorite and kaolinite) and the Deccan Traps (smectite). The wavelet and cross-spectral analyses further reveal that sediment transport to the eastern Arabian Sea since 600 kyr is mainly dominated by sea-level variations in the eccentricity (100-kyr) band, while the Indian summer monsoon might contribute moderately to the precession (23-kyr) band. The  $\delta^{15}\text{N}$  and turbidite frequency indicate that more turbidite events are associated with Indus River-sourced sediments at IODP Site U1457 during sea-level lowstands, which might reflect a reconnection of deep-sea channels to the Indus River mouth and/or reworking of previously deposited Indus River sediments located northward.

**Key words:** Arabian Sea Monsoon; Expedition 355; sea level; Indus River; Deccan Traps; IODP Site U1457.

## 1. Introduction

Deep-sea fans receive large amounts of sediment transported from terrigenous sources by canyon-channel systems, rivers, ocean currents and/or winds. Studies of sediment dynamics reveal that the interaction of continental weathering inputs (mainly fluvial and eolian inputs), tectonic activity and sea-level variations control the amount of sediment deposited on the deep-sea fans (Peizhen et al., 2001; Prins and Postma, 2000; Steinke et al., 2003). Over the Late Quaternary, the impacts of continental weathering inputs and sea-level variations on sediment transport processes can be better addressed when tectonic uplift can be ignored (An et al., 2001; Colin et al., 2010; Jousain et al., 2016). Therefore, Quaternary sediments deposited in deep-sea fans have been investigated to reconstruct the past changes of paleoenvironment and paleoclimate in the sediment source region (Caley et al., 2011; Clift et al., 2008; Jousain et al., 2017; Wan et al., 2012) and the sediment transport processes (Bourget et al., 2010; Prins and Postma, 2000; Steinke et al., 2008). First, sediments delivered from the continent to the ocean are related to the sediments produced by the intensity of erosion/alteration and their transportation in the fluvial systems (Castelltort and Van Den Driessche, 2003; Milliman and Meade, 1983). Such sediment input is probably enhanced during periods of increased precipitation with respect to the influence of vegetation and geomorphology (West et al., 2005; White and Blum, 1995). In low-latitude regions, the monsoon plays a key role in regulating the local climate (Webster, 1987) and controlling the sediment yield/discharge (Milliman and Meade, 1983; Unger et al., 2003). The monsoon-induced rainfall intensity greatly influences fluvial dynamics and consequently has an impact on the nature and timing of sediment delivery to the sea (Webster, 1987; Yu et al., 2017). Additionally, the seasonal reversal of the wind-driven sea surface circulation also has the potential to alter the mode and intensity of sediment transport to the ocean (Colin et al., 1999; Liu et al., 2003). Second, sea-level variations during the Quaternary have a great impact on the degree of sediment dynamics (Posamentier and Vail, 1988; Steinke et al., 2008). During sea-level lowstands, the fluvial systems directly feed the coastlines and enhance the transport of detrital sediment to the ocean (Bourget et al., 2010; Posamentier and Vail, 1988). Inversely, sea-level highstands can drown the continental shelf, resulting in sediment partitioning and reducing the amount of coarse sediment transferred towards the deep ocean (Bourget et al., 2010; Posamentier and Vail, 1988).

Recent studies have demonstrated that deep-sea sediment records of the Bengal Fan and the South China Sea are suitable to reconstruct weathering of the Himalayan river basins and sediment transfer from land to sea during the Late Quaternary (Colin et al., 1999; Fournier et al., 2017; Jousain et al., 2017; Liu et al., 2004; Wan et al., 2015; Yu et al., 2016). These studies indicate that

the weathering and transport of sediments from land to sea by the Ganga-Brahmaputra river system and the Mekong River are very sensitive to climate changes such as monsoon rainfall and to sea-level variations. Investigations of the Late Quaternary turbidite system growth along the Makran convergent margin reveal a complex interplay of tectonics, climate and sea-level variations in controlling the input of terrigenous sediment (Bernhardt et al., 2017; Bourget et al., 2010; Prins et al., 2000b). From a source-to-sink perspective, the amount and timing of sediment transfer from the Makran continent to the northern Arabian Sea varied in response to changes including sediment production in the drainage basin, the capacity of transport from fluvial systems (monsoon), and sediment trapping and sorting on the shelf area (sea level) (Bourget et al., 2010; Prins et al., 2000b). The turbidity deposits as well as the sand-to-mud ratio in the deep Indus Fan are likely determined by monsoon changes in the sediment source area (Bourget et al., 2010; Caley et al., 2011). Furthermore, sediment cores from the Indus Canyon and the middle Indus Fan in the Arabian Sea indicate that both sea-level changes and monsoon-induced differences have influenced the sediment supply and deposition over the past 20 kyr (Prins and Postma, 2000). While it is hypothesized that the monsoon climate and sea-level variations have controlled the erosional and depositional cycles since the late glacial period (Bourget et al., 2013; Prins and Postma, 2000; Steinke et al., 2008), their relative importance has not been assessed at millennial timescale over the glacial-interglacial cycles. In the specific case of the Arabian Sea, where the Indus Fan system is characterized by one of the highest sediment deposition rates in the world, orbital controls on sediment transfer and dispersion in the ocean have rarely been reported (Bourget et al., 2010; Prins et al., 2000b). Coincidentally, such records are also limited from other marginal seas fed by inputs of extensive continental weathering, such as the Bay of Bengal (Colin et al., 2006; Joussain et al., 2017), the South China Sea (Liu et al., 2003; Steinke et al., 2006; Wan et al., 2010), and the East China Sea (Gao and Collins, 2014; Li et al., 2014). In addition, in the northern Arabian Sea, it has been demonstrated that eolian dust could be significant for deep-sea sedimentation and help to reconstruct the past dynamics of wind system links with the summer and winter Indian monsoon intensities (Clemens and Prell, 1990; Pourmand et al., 2004; Prins and Weltje, 1999). Therefore, the Quaternary sediments of the Indus Fan have great potential to constrain the effects of monsoon climate and sea-level variations on sediment transfer to the eastern Arabian Sea.

In this study, for the first time, we conducted high-resolution ( $\approx 2$  kyr) clay mineral and Sr-Nd isotopic measurements on the sediments of IODP Site U1457 located in the Laxmi Basin over the last 600 kyr to (i) reconstruct the temporal variability of sediment sources and (ii) constrain the

impacts of climate (Indian monsoon rainfall) and sea-level changes on the dynamics of sediment export to the Indus Fan at orbital timescales.

## **2. Regional setting**

A seasonal reversal of the surface circulation in the Arabian Sea is dominated by the Indian monsoon (Fig. 1) (Shetye et al., 1994). The bottom water (deeper than about 3500 m) in the Arabian Sea is generally supplied by Antarctic Bottom Water (AABW) and North Atlantic Deep Water (NADW) which move northward and upwell mixing with North Indian Deep Water (NIDW: approximately 1500–3500m) (Fig. 1) (Shetye et al., 1994). The Indus deep-sea Fan is one of the largest submarine fans in the world (1600 km N-S and 1000 km E-W) (McHargue and Webb, 1986). It is mainly fed in the north by the Indus River that drains the western Himalayas, which have one of the world's highest physical and chemical erosion rates (Milliman and Meade, 1983; Sarin et al., 1989). At present, most of the sediments from the Indus River are transferred to the Indus Fan by a submarine canyon in the western Arabian Sea (Prins et al., 2000a). The Deccan Traps is one of the largest basaltic provinces on the Earth (Dessert et al., 2001). It is located in the western and central parts of India (Fig. 1). The region of the Deccan Traps is dominated by a monsoonal climate, with a heavy annual rainfall of 1000-3000 mm, the major part of which arrives during the summer season between June and September (Kripalani and Kulkarni, 2001). The annual mean temperature is 25°C, with a maximum of 35°C in May (Dessert et al., 2001; Singh and Gupta, 2013). Sediments from the Deccan Traps are mainly transported by the Sabarmati, Mahi, Narmada and Tapi Rivers to the Arabian Sea. The main sedimentary sources feeding the eastern Indus Fan are the rivers from the Indus basin (Indus River) and the Deccan Traps (Sabarmati, Mahi, Narmada and Tapi Rivers) (Kessarkar et al., 2003). The Indus River is one of the world's largest rivers in terms of drainage (970000 km<sup>2</sup>) and water discharge (243 km<sup>3</sup>) (Haq and Milliman, 1984). It mainly drains the arid to semi-arid Western Himalaya Mountains, with headwaters higher than 4000 m. Approximately 100 million tons of sediment is transferred to the Indus Fan annually, of which >80% is transported during the summer monsoon period (Milliman and Meade, 1983). The total sediment discharge of the Sabarmati, Mahi, Narmada and Tapi Rivers draining the Deccan Traps also yields ~100 million tons per year (Alagarsamy and Zhang, 2005). In addition to these amounts, ~100 million tons of eolian dust sourced from Oman, Africa and the western India deserts is transported to the Arabian Sea by wind annually. However, only ~30 million tons arrive in the eastern Arabian Sea, which may further decrease toward the southeast Arabian Sea (Ramaswamy and Nair, 1994; Sirocko and Sarin, 1989).

### 3. Materials and methods

#### 3.1 Core description and age model

The IODP Site U1457 (17°9.95'N, 67°55.80'E, water depth 3534 m) was drilled in the Laxmi Basin located in the eastern part of the Indus Fan during IODP Expedition 355 (Fig. 1). IODP Site U1457 is located ~490 km west of the Indian coast and ~760 km south from the present-day Indus River mouth. In this study, we have investigated the upper 43 mbsf of IODP site U1457 corresponding to the last 600 kyr (Pandey et al., 2015). The lithology of the studied sections consists of light brown to light green nannofossil ooze including foraminifer-rich nannofossil ooze and nannofossil-rich clay, interbedded with silty clay and silty sand (Pandey et al., 2015). The silty sand layers display normal grading and sharp erosive bases and correspond to turbidite layers. The hemipelagic nannofossil ooze and nannofossil-rich clay show intense burrowing and frequently include pyrite nodules and veins. Quartz, feldspar, and mica grains are common, whereas heavy minerals (hornblende, clinopyroxene, epidote, garnet, and augite) are rare.

The age model of IODP Site U1457 is based on stable oxygen isotopic record ( $\delta^{18}\text{O}$ ) obtained from surface dwelling planktic foraminifera *Globigerinoides ruber*, biostratigraphy and paleomagnetic data (Saraswat et al., unpublished data). This  $\delta^{18}\text{O}$  data of IODP U1457 was also compared and tuned to the global benthic LR04 record (Lisiecki and Raymo, 2005). Detailed comparison of  $\delta^{18}\text{O}$  record from IODP Site U1457 with the global benthic LR04 is shown in figure 2. The age model error of IODP Site U1457 is approximately 4 kyr as introduced from the LR04 record for the last 1 Ma interval (Saraswat et al., unpublished data). According to the age model, the upper 43 mbsf of IODP Site U1457 provides a continuous record of the last 600 kyr, with an average linear sedimentation rate (LSR) of approximately 7.2 cm/kyr (ranging from 2 to 16.4 cm/kyr).

#### 3.2 Clay mineral X-ray diffraction (XRD)

A total of 257 samples collected from the top 43 mbsf of IODP site U1457 were used for clay mineralogical analyses, permitting us to obtain a mean time resolution of 2.3 kyr. The clay minerals were identified by X-ray diffraction (XRD) using a PANalytical diffractometer at the GEOPS laboratory (Université Paris-Saclay, France) on oriented mounts of non-calcareous clay-sized (<2  $\mu\text{m}$ ) particles. Briefly, deflocculation was accomplished by successive washing (about 5 rinse cycles) with distilled water after removing carbonate and organic matter by treating with acetic acid (25%) and hydrogen peroxide (15%), respectively.

The particles smaller than 2  $\mu\text{m}$  were separated by sedimentation and centrifugation. Three XRD runs were performed, following air-drying, ethylene-glycol solvation for 24 hours, and heating at 490°C for 2 hours. The clay minerals were identified according to the position of the (001) series of basal reflections on the three XRD diagrams. Mixed layers composed mainly of smectite-illite (15–17 Å) were included in the “smectite” category. Semi-quantitative estimates of peak areas of the basal reflections for the main clay mineral groups of smectite (15–17 Å), illite (10 Å), and kaolinite/chlorite (7 Å) were performed on the glycolated curve using the MacDiff software. The relative proportions of kaolinite and chlorite were determined based on the ratio from the 3.57/3.54 Å peak areas. The replicate analyses of a few selected samples gave a precision of  $\pm 2\%$  (2 $\sigma$ ). Based on the XRD method, the semi-quantitative evaluation of each clay mineral had an accuracy of  $\sim 4\%$ . Additionally, illite crystallinity was obtained from the half-height width of the 10 Å peak on the glycolated curve. The lower values represent higher crystallinity, characteristic of weak hydrolysis in continental sources and cold, arid climate conditions (Chamley, 1989). The illite chemistry index, referring to the ratio of the 5 Å and 10 Å peak areas (Esquevin, 1969), was also calculated. Illite with chemistry index lower than 0.15 (Fe-Mg rich) is considered to have formed in an environment with intense physical weathering, while illite with a chemistry index higher than 0.4 is usually Al-rich and formed by strong chemical hydrolysis (Petschick et al., 1996).

### **3.3 Radiogenic isotope and grain-size determinations**

The Sr-Nd isotopic compositions and grain-size were determined for thirty-five carbonate and organic matter-free sediments. Bulk sediment was treated with acetic acid (25%) and hydrogen peroxide (15%) in order to remove carbonate and organic matter, respectively. Then part of the sample was separated for grain-size measurement on a Malvern Mastersizer X at the GEOPS laboratory (Université Paris-Saclay, France). The measurement reproducibility is better than 2%. The remaining sample was first dissolved in hydrofluoric acid (HF) and HNO<sub>3</sub>-HCl mixtures. An initial chemical separation used Bio-Rad columns packed with AG50W X-8, 200-400 mesh cationic exchange resin. Sr and REE were isolated using 2 N HCl and 2.5 N HNO<sub>3</sub>, respectively. The Sr fraction was purified on a 20-ml Sr Spec column consisting of a polyethylene syringe with a 4 mm  $\varnothing$  Millex filter. Nd was extracted and purified from the REE fraction using a Ln Spec column following the method described in detail by Copard et al. (2010). In this method, samples were loaded using 0.7 ml of 0.05 N HNO<sub>3</sub> on preconditioned Ln Spec columns. The unwanted cations were eluted using 3.25 ml of 0.25 N HCl. Nd was then eluted with an additional 2.5 ml of 0.25 N HCl. Sr and Nd isotopic compositions were analyzed using a Thermo Scientific Multi-Collector Induced Coupled Plasma Mass Spectrometer (MC-ICP-MS NEPTUNE Plus) at the Laboratoire des

Sciences du Climat et de l'Environnement (LSCE) in Gif-sur-Yvette. The Sr and Nd isotopic compositions were analyzed at concentrations of 15 to 20 ppb. During the analytical sessions, every two samples were bracketed with analyses of appropriate Sr standard solution NIST SRM987 characterized by a certified value of 0.710250. For the Nd isotopic composition analyses, samples were bracketed by using Nd standard solutions JNdi-1 and La Jolla characterized by certified values of  $0.512115 \pm 0.000006$  and  $0.511858 \pm 0.000007$ , respectively (Lugmair et al., 1983; Tanaka et al., 2000). Standard solutions were analyzed at concentrations similar to those of the samples. The mass-fractionation correction was made by normalizing  $^{146}\text{Nd}/^{144}\text{Nd}$  to 0.7219 and  $^{86}\text{Sr}/^{88}\text{Sr}$  to 0.1194 and applying an exponential fractionation correction. Nd results are expressed as  $\epsilon\text{Nd}(0) = [((^{143}\text{Nd}/^{144}\text{Nd}_{\text{meas}})/0.512638) - 1] \times 10000$ , using the CHUR value given by Jacobsen and Wasserburg (1980).

### **3.4 Spectral analysis**

Continuous wavelet transform of the selected data was performed using MATLAB. All the data was filtered with a 10-150 kyr bandpass. All records were linearly interpolated to the average sample spacing of the record concerned. This wavelet software is available at: <http://paos.colorado.edu/research/wavelets/> (Torrence and Compo, 1998). A significance level of 95% was adopted when the results are exported. Cross-spectral analysis was adopted by Arand software to statistically compare the difference of physical relationships between the potential forcing mechanisms and climate response. This software is available at: <https://www1.ncdc.noaa.gov/pub/data/paleo/softlib/>. A bandwidth for 300 lags was used for this study. Both significance level of 80% and 95% were adopted in the exported result

## **4. Results**

### **4.1 Clay mineralogy**

The clay mineral assemblage of IODP Site U1457 (reported as supplementary data) is mainly composed of smectite (10-86%, average 57%) and illite (9-62%, average 28%), while chlorite (3-23%, average 12%) and kaolinite (1-8%, average 3%) are less abundant (Fig. 3). Smectite variations are inversely correlated with illite, chlorite and kaolinite distributions owing to the “closed sum” effect (Fig. 3). The clay mineral percentages exhibit approximate glacial–interglacial cycles. In general, smectite is relatively higher during interglacial marine isotope stages (MIS), particularly in MIS 1, 7, 9, 11, 13 and 15. Illite, chlorite and kaolinite contents mostly display higher values during glacial MIS 2, 6, 10, and 14. Such glacial–interglacial cycles are particularly well marked between 600 and 150 kyr but become less obvious from 150 kyr to the present. Considering that the smectite

distribution is inversely correlated with those of illite, chlorite and kaolinite, the smectite/(illite+chlorite) ratio has been reported in Figure 2 3 to represent mineralogical changes within the clay fraction. Variations of this mineralogical ratio range from 0.3 to 9.5 and are similar to those obtained for smectite contents. The illite chemical index presents a moderate range of variations between 0.18 and 0.33, with an average of 0.18 (Fig. 3). The crystallinity of illite varies between 0.12 and 0.32°  $\Delta 2\theta$  (with an average value of 0.19°  $\Delta 2\theta$ ). No clear glacial–interglacial cycles are observed in the illite chemical index or in the illite crystallinity (Fig. 3).

## **4.2 Sr-Nd isotopic compositions**

$^{87}\text{Sr}/^{86}\text{Sr}$  ratios and  $\epsilon\text{Nd}$  values, measured on the detrital fraction of 35 samples from IODP Site U1457, are reported in Table 1.  $^{87}\text{Sr}/^{86}\text{Sr}$  ratios and  $\epsilon\text{Nd}$  values have been measured in hemipelagic sediments and in turbidite deposits identified by visual description. For hemipelagic sediments,  $^{87}\text{Sr}/^{86}\text{Sr}$  ratios and  $\epsilon\text{Nd}$  values are characterized by wide ranges from 0.7154 to 0.7255 and from -12.9 to -9.5, respectively. Three samples collected in turbidite layers have been analyzed in the last 600 kyr (Table 1). The  $\epsilon\text{Nd}$  values and  $^{87}\text{Sr}/^{86}\text{Sr}$  ratios of these turbidity layers are generally different from those of the hemipelagic sediments with systematically more negative  $\epsilon\text{Nd}$  values (from -13.0 to -13.7) and similar  $^{87}\text{Sr}/^{86}\text{Sr}$  ratios (from 0.7197 to 0.7209).

## **5. Discussion**

### **5.1 Sources of sediments and clay minerals to IODP Site U1457**

IODP Site U1457 exhibits large glacial and interglacial variations in the smectite/(illite+chlorite) ratio. The interpretation of such mineralogical records requires knowledge of the potential source areas as well as of the mode and strength of the transport processes involved. Previous studies have shown that mineralogy of the clay-size fraction combined with Sr-Nd isotopic compositions of deep-sea sediments from the Arabian Sea is suitable to establish the main sedimentary sources feeding the Indus Fan (Goswami et al., 2012; Kessarkar et al., 2003). The applicability of the clay mineralogy and Sr-Nd isotopic ratios for provenance studies arises from the fact that the potential sediment sources (eolian dust, Indus River, rivers from the volcanic province of the Deccan Traps and the Peninsular Gneissic Rock) are characterized by contrasting mineralogical and geochemical signatures (Goswami et al., 2012; Kessarkar et al., 2003).

#### **5.1.1 Sr-Nd isotopic compositions**

In this study, Sr-Nd isotopic composition of detrital sediments from IODP Site U1457 is supposed to represent the origin of the siliciclastic fraction from its sources. No significant correlations between



mean grain-size versus  $87\text{Sr}/86\text{Sr}$  (Fig. 4a) and  $\epsilon\text{Nd}$  (Fig. 4b) are observed, suggesting that the grain size effect should be insignificant for the study site. Considering the anti-related role of  $87\text{Sr}/86\text{Sr}$  and  $\epsilon\text{Nd}$ , we mainly attribute the changes of Sr isotopes ratio here to the variation of sediment sources to IODP Site U1457. Such interpretation is consistent with studies of marine sediment cores in South China Sea (Wan et al., 2017) and West Philippine Sea (Xu et al., 2018).  $\epsilon\text{Nd}$  and  $\delta^{13}\text{C}$  records from core SK129–CR2 in the equatorial Indian Ocean indicated that the variations of northern Indian deep-water circulation are induced by increased proportion of NADW during interglacials and reduced proportion during glacials while the variation of AABW is unimportant (Piotrowski et al., 2009). The  $\epsilon\text{Nd}$  of NADW is generally stable at  $\sim -13$  during glacials and interglacials (Howe et al., 2016). If variations of NADW supply have largely influenced the glacial-interglacial  $\epsilon\text{Nd}$  offset observed in our record, one should expect a  $\epsilon\text{Nd}$  shift towards  $-13$  during interglacials as the proportion of NADW arrived in the northern Indian Ocean increase during interglacials. However, our  $\epsilon\text{Nd}$  data indicate the opposite (Fig. 4 and 5). Such contrasting observation suggests that the authigenic Fe-Mn oxyhydroxide coatings formed inside the Arabian Sea have a less pronounced influence on the obtained  $\epsilon\text{Nd}$  of our detrital sediment. Moreover, the glacial-interglacial  $\epsilon\text{Nd}$  offset observed in the detrital sediment of IODP Site U1457 cannot be simply explained by changes in deep-water circulation. To better constrain the sedimentary sources, we have reported in an  $\epsilon\text{Nd}$  versus  $87\text{Sr}/86\text{Sr}$  diagram results obtained on detrital samples from IODP Site U1457 (Fig. 4c) together with (i) sediments from the eastern Arabian shelf core SS-3104G (Goswami et al., 2012); (ii) sediments from Indus delta cores Indus-10 NW Shelf and Indus-23 Clinoform (Limmer et al., 2012); and (iii) eolian dusts from north Africa and central Arabia (Grousset and Biscaye, 2005; Scheuven et al., 2013). A major contribution of eolian particles from the Arabian peninsula ( $87\text{Sr}/86\text{Sr}$  from 0.71 to 0.73;  $\epsilon\text{Nd}$  from 2 to 6) (Stein and Goldstein, 1996; Stoesser and Frost, 2006) to the IODP Site U1457 can be excluded by the distinct  $\epsilon\text{Nd}$  (Fig. 4c). A portion of dust from northeast Africa (southern Egypt, northern Sudan) has Sr-Nd isotopic composition similar to that of sediments from IODP Site U1457 and cannot be omitted based only on such isotopic composition (Grousset and Biscaye, 2005; Scheuven et al., 2013). However, several studies have shown that eolian dust derived from the north Africa and Arabian deserts (Tateo et al., 2000; Verrecchia and Coustumer, 1996a) and deposited in the western and northern Arabian Sea is relatively rich in palygorskite (2-10%) and to a lesser extent in sepiolite (Kolla et al., 1981; Scheuven et al., 2013; Sirocko and Lange, 1991). This mineral is transported principally by winds and is particularly abundant in Arabian Peninsula soils (Mackenzie et al., 1984; Shadfan and Mashhady, 1985; Verrecchia and Coustumer, 1996b). The absence of palygorskite in IODP Site

U1457 sediments suggests an insignificant eolian contribution to the Laxmi Basin sediments at least for the last 600 kyr. Consequently, considering the great distance from the Arabian deserts to IODP Site U1457, the absence of palygorskite and the relatively small amount of eolian flux compared with the annual river inputs to the eastern Arabian Sea (~30 million tons eolian versus ~200 million tons of river inputs from the Indus 332 basin and Deccan Traps), we can reasonably hypothesize that eolian contributions from North 333 African and Arabian deserts may be slight. Such a result is in agreement with previous studies that indicated negligible eolian contribution in the eastern Arabian Sea sediments (Goswami et al., 2012; Kessarkar et al., 2003). In addition, sediments from Gneissic Rock of the southern Indian continent display  $^{87}\text{Sr}/^{86}\text{Sr}$  from 0.71 to 0.73 and  $\epsilon\text{Nd}$  from -25 to -20 (Goswami et al., 2012), which are distinct from sediments of IODP Site U1457 ( $^{87}\text{Sr}/^{86}\text{Sr}$  from 0.7154 to 0.7255 and  $\epsilon\text{Nd}$  from -13.7 to -9.5, this study). Such distinct  $\epsilon\text{Nd}$  results indicate that Gneissic Rock of the southern Indian continent has a minor contribution to IODP Site U1457. It has been shown that the Sr and Nd isotopic compositions of the Indus River sediments are very different from the modern ( $^{87}\text{Sr}/^{86}\text{Sr}$  from 0.730 to 0.735;  $\epsilon\text{Nd}$  from -15 to -12) (Clift et al., 2008; Kessarkar et al., 2003) and last glacial maximum (LGM) sediments ( $^{87}\text{Sr}/^{86}\text{Sr}$  from 0.710 to 0.715;  $\epsilon\text{Nd}$  from -12.5 to -10) (Clift et al., 2010). Consequently, in Figure 3a4a, we have reported the mixing lines between three potential sedimentary sources: the Deccan Traps (Goswami et al., 2012; Lightfoot and Hawkesworth, 1988), the modern Indus River (Kessarkar et al., 2003) and the LGM Indus River (Clift et al., 2010). The  $\epsilon\text{Nd}$  and  $^{87}\text{Sr}/^{86}\text{Sr}$  ratio analyzed for glacial and interglacial hemipelagic sediments from IODP Site U1457 plot mainly along a mixing curve between two end members corresponding to the modern Indus River sediments and the Deccan Traps. Such results do not confirm a strong change of the Sr-Nd isotopic composition of sediments from the Indus River during glacial periods (LGM). However, the reason of glacial–interglacial changes of Indus River end-member is not clear given that the sediment source of the Indus River has generally been stable despite the climate variation since the Late Quaternary (Alizai et al., 2012; Clift et al., 2010). The  $\epsilon\text{Nd}$  and  $^{87}\text{Sr}/^{86}\text{Sr}$  ratios indicate that interglacial sediments are associated with a relatively higher proportion of sediments derived from rivers that drain the Deccan Traps ( $^{87}\text{Sr}/^{86}\text{Sr}$  from 0.707 to 0.714;  $\epsilon\text{Nd}$  from -6 to -3) (Dessert et al., 2001; Lightfoot and Hawkesworth, 1988), with a contribution from 40 to 60% calculated from simple two end member mixing (Fig. 4c). Meanwhile, glacial sediments are characterized by a relatively higher proportion of sediments derived from the modern Indus River, with a contribution from 45 to 80% (Fig. 4c).

### 5.1.2 Clay mineralogy

Previous studies have shown that clay minerals transported to the eastern Arabian Sea originate mainly from the Indus River, Deccan Traps and the Peninsular Gneissic Rock of the southern Indian continent (Fig. 1) (Clift et al., 2001; Kessarkar et al., 2003; Kolla et al., 1981; Prins et al., 2000a). The Indus River is influenced by the southwest monsoon, with sediments derived from the western Himalaya and Karakoram. The Indus sediments have a uniformly low proportion of kaolinite (2-6%) and a wide range of smectite (20-52%) versus physically weathered illite and chlorite (41-64%) (Alizai et al., 2012; Kolla et al., 1981). Furthermore, illite and chlorite proportions are approximately 10% higher in the Indus delta sediments than in the Indus basin (Alizai et al., 2012). Both illite and chlorite are considered primary minerals that result mainly from intensive physical erosion and moderate chemical weathering of metamorphic (i.e., muscovite or biotite) and granitic parent rocks but can also be derived from reworking of sedimentary rocks (Chamley, 1989). In the western Himalayan area, sediments are mainly produced in the highlands of the river basins by physical erosion (Alizai et al., 2012). For IODP Site U1457, the illite chemical index (between 0.08 and 0.33, average 0.18) is characterized by a narrow range of relatively low values implying abundant Fe-Mg-rich illite formed under poor hydrolysis conditions (Ehrmann, 1998) and could indicate a stable sedimentary source for the mineral illite through time. Such results are compatible with sedimentary sources located in the highlands of the Himalayas without the strong chemical weathering in plain soils (Galy and France-Lanord, 2001; Joussain et al., 2017). The Deccan Traps area is dominated by a subtropical Asian monsoonal climate. Smectite is considered as a secondary mineral produced by the chemical weathering of parent aluminosilicates and ferromagnesian silicates under warm and seasonally contrasting climatic conditions (Biscaye, 1965; Chamley, 1989). The clay mineral assemblage of soil formed on the Deccan Traps basalts indicates large amounts of smectite (60-100%, average approximately 80%) (Bhattacharyya et al., 1993; Keller et al., 2009; Rao and Rao, 1995). The higher smectite/(illite+chlorite) ratios during interglacial periods are generally synchronous with radiogenic  $\epsilon_{\text{Nd}}$  values (Fig. 5a), suggesting that smectite is mainly derived from the volcanic province of the Deccan Traps. Considering the position of IODP Site 1457, it is reasonable to hypothesize that sediment input from the Deccan Traps area is responsible for the predominance of smectite associated with minor kaolinite in the clay mineral assemblage of IODP Site U1457 (Fig. 4d). Such a conclusion is consistent with previous studies on marine cores located in the eastern Arabian Sea, which show that sediments derived from the Deccan Traps are rich in smectite (23-76%), illite and chlorite (17-54%) but are poor in kaolinite (7-10%) (Kessarkar et al., 2003; Phillips et al., 2014). In addition, the Peninsular Gneissic Rock in the southern Indian continent is characterized by a humid tropical climate and intense chemical weathering (Das et al.,

2005). The clay mineral compositions of sediments from the southern Indian continent indicate plentiful illite and chlorite (46-58%) and moderate smectite (24-34%) and kaolinite (19-27%) (Kessarkar et al., 2003). Hence, a strong contribution of sediments from Gneissic Rock of the southern Indian continent to IODP Site U1457 can be excluded due to its distinct clay mineralogy (high kaolinite content, Fig. 4d) and  $\epsilon\text{Nd}$  values ( $^{87}\text{Sr}/^{86}\text{Sr}$  from 0.71 to 0.73;  $\epsilon\text{Nd}$  from -25 to -20) (Goswami et al., 2012). Such a conclusion is also supported by previous cores studied along the western margin of India, which indicate a negligible contribution from the southern Indian continent to the Laxmi basin (Kessarkar et al., 2003). Therefore, variations in the clay mineralogy of IODP Site U1457 result mainly from the mixing of detrital material deriving from the Indus River (illite, chlorite and kaolinite) and from erosion of the Deccan Traps (smectite). Smectite derived from the large volcanic province of the Deccan Traps could reach our study site through several rivers (such as the Tapi, Mahi and Marmada Rivers, Fig. 1) and marginal currents. Sediments from the Indus River could also be transported, mainly to the eastern Arabian Sea, by the southerly current driven by the southwest monsoon (Fig. 1) (Kessarkar et al., 2003). Consequently, the smectite/(illite+chlorite) ratio can be used to reconstruct past variations in the relative proportion of sediments derived from the Indus River and rivers draining the Deccan Traps. The variations of the smectite/(illite+chlorite) ratio are generally consistent with  $\epsilon\text{Nd}$  values and magnetic susceptibility from IODP Site U1457, all of which fluctuate at glacial–interglacial cycles (Fig. 5a, b). During the interglacial periods (sea-level highstands), higher smectite/(illite+chlorite) ratios correspond to more radiogenic detrital  $\epsilon\text{Nd}$  values and higher magnetic susceptibility. Inversely, glacial periods and cold substages of the interglacial periods (sea-level lowstands) are characterized by lower smectite/(illite+chlorite) ratios, less radiogenic detrital  $\epsilon\text{Nd}$  values and lower magnetic susceptibility, despite some discrepancies during MIS 8 and 12. Such results suggest that a higher proportion of detrital sediments deriving from the volcanic province with positive  $\epsilon\text{Nd}$  values and high smectite/(illite+chlorite) ratios is also associated with higher magnetic susceptibility. In general, magnetic susceptibility carries an intrinsic signal that depends on concentration, grain size and type of magnetic mineral, which can reflect subtle variations of the sedimentary sources and/or the dynamics of sediment transport (Heller and Liu, 1982; King and Channell, 1991). It has been shown that the weathering of tholeiitic basalts (within the Deccan Traps, at least 95% of the lavas are tholeiitic basalts) in the Deccan Traps mainly produces pedogenetic 432 phyllosilicates (e.g., kaolinite and the smectite group minerals) and Fe and Mn oxides or 433 oxyhydroxides, which are generally characterized by higher magnetic susceptibility (Babechuk et al., 2014). The magnetic susceptibility record is hardly affected by diagenetic processes as it behaves consistently with those proxies (smectite content and  $\epsilon\text{Nd}$ ) which

are not strongly affected by diagenetic processes in the last 600 kyr. Consequently, considering that the magnetic mineralogy does not change drastically in the last 600 kyr of IODP site U1457, the magnetic susceptibility can permit us to track the relative contribution of sediments deriving from the Deccan Traps at higher temporal resolution than the record of smectite/(illite+chlorite) ratio. Nevertheless, further investigations of the magnetic mineralogy of IODP Site U1457 sediments would be necessary to constrain the factors that control the magnetic susceptibility variations.

## **5.2 Climatic impacts on sedimentation of the eastern Arabian Sea**

Variations in the proportion of sediments deriving from the Indus River and from rivers draining the Deccan Traps as reconstructed by the smectite/(illite+chlorite) ratio and magnetic susceptibility from IODP Site U1457 could be influenced by both changes in the intensity of the Indian monsoon and sea-level variations. Changes in the Indian monsoon rainfall could modify the vegetation cover, runoff, erosion and weathering rate in the Indus basin and thus the subsequent sediment transfer to the Indus Fan. Such a conclusion has been highlighted by sedimentological and geomorphologic studies of deep-water turbidite system in the Makran convergent margin (Bourget et al., 2010; Prins and Postma, 2000). In addition, the dynamics of sediment transport and the distribution of sediments in the Arabian Sea could be modified by oceanic surface circulation, which is mainly driven by the monsoon wind (Beal et al., 2014). To evaluate the impact of changes in the intensity of the Indian summer monsoon, we report in Figure 4d 5d the Indian summer monsoon wind strength as reconstructed by lithogenic grain size of ODP Site 722 (Clemens et al., 1996) and insolation at 30°N in June (Laskar et al., 2004). The Indian summer monsoon is marked by strong southwest winds over the Arabian Sea, which are driven by atmospheric heating and the difference between the Asian low-pressure cell and the southern subtropical Indian Ocean high-pressure cell (Webster, 1987). The lithogenic grain size record of ODP Site 722 located in the western Arabian Sea can be used to monitor the transport capacity of the summer southwest winds (larger values correspond to stronger winds) associated with the strength of the Asian low-pressure cell (Clemens et al., 1996). This record is well correlated with upwelling-induced productivity proxies (opal flux and *G. bulloides* %) in the Arabian Sea (Clemens et al., 1996). There is a good correlation between the lithogenic grain size record and the insolation curve calculated at 30°N in June (Fig. 5d). Such a result is not surprising given that both of them are directly linked to the precession modulated by the eccentricity (Clemens et al., 1996; Laskar et al., 2004). However, the smectite/(illite+chlorite) ratios as well as the magnetic susceptibility indicate no direct link to the Indian summer monsoon wind strength (Fig. 5), suggesting a weak influence of the Indian summer monsoon on the sediment delivered to IODP Site U1457. The sea-level variation has the potential to i) rework sediment previously deposited in the

Arabian Sea plains and continental shelves and ii) modify the connection between the river mouth and the head of the Indus Fan deep-sea channels (Bourget et al., 2010; Prins et al., 2000a; Steinke et al., 2008). The glacial–interglacial variations observed in the smectite/(illite+chlorite) ratios as well as in the magnetic susceptibility curve are relatively well correlated to the stacked global benthic  $\delta^{18}\text{O}$  record of LR04 (Lisiecki and Raymo, 2005) and global sea-level variation (Bintanja et al., 2005) (Fig. 5). Such results suggest that changes in the relative proportion of sediments originating from the Indus River and Deccan Traps are largely controlled by sea-level changes. In the East Asia marginal seas (such as the South China Sea), it is important to decipher the effect of changes in the East Asian monsoon and sea-level variations on the orbital timescale sediment dynamics during the Quaternary (Li et al., 2014; Liu et al., 2015; Steinke et al., 2006). Both the East Asian monsoon and sea level indicate a dominant eccentricity band (100-kyr) and moderate obliquity (41-kyr) and precession cycles (23- and 19-kyr) in particular during the Late Quaternary (Liu et al., 2003; Wan et al., 2012; Yu et al., 2016). However, this is not the case in the Arabian Sea and the Bay of Bengal, both of which are mainly influenced by the Indian monsoon system. While the glacial– interglacial sea level is globally consistent, with strong eccentricity cycles, the intensity of the Indian summer monsoon is mainly forced by the obliquity and precession, modulated by the eccentricity (Caley et al., 2011; Clemens and Prell, 2003). Such a character of the Indian summer monsoon intensity could be due to the obliquity and precession cycles, as they maximize strong interhemispheric transport (An et al., 2011; Clemens and Prell, 2003). Therefore, it is possible to use this specific character to constrain their different influence on sediment transport in the Arabian Sea. The long-term smectite/(illite+chlorite) record since 600 kyr ago from IODP Site U1457 offers a good opportunity to evaluate the relative effects of the Indian summer monsoon and sea-level variations on sediment transfer to the eastern Arabian Sea. Wavelet transforms of a) the smectite/(illite+chlorite) ratio from IODP Site U1457 (this study), b) sea level (Bintanja et al., 2005) and c) the Indian summer monsoon wind 501 strength (Clemens et al., 1996) are performed to indicate the dominant orbital cycle through the last 600 kyr (Fig. 6). The cross-spectral relationships between the smectite/(illite+chlorite) ratio from IODP Site U1457 (this study) and a) sea level (Bintanja et al., 2005) and b) Indian summer monsoon wind strength (Clemens et al., 1996) are also applied to compare their frequency domains (Fig. 7). The cross-spectral analysis allows one to statistically constrain the potential initiative and responsive mechanism of periodic spectra from different records (Clemens et al., 1996). Here, we use the cross-spectral analysis to exam the orbital driving of sea level or Indian summer monsoon wind on the smectite/(illite+chlorite) ratio. The smectite/(illite+chlorite) ratio and sea-level variation reveal similar spectra (strong 100-kyr with

weak 41-kyr and 23-kyr periodicities throughout the last 600 kyr). The strong eccentricity band is also highlighted in their cross-spectral analysis with a non-zero coherency greater than 95% (Fig. 7a), suggesting a robust forcing of sea level on the clay mineralogical ratio and sediment balance from the Deccan Traps and the Indus River in IODP Site U1457 during the last 600 kyr. However, correlations between the 41-kyr cycle and particularly the 23-kyr cycle of the smectite/(illite+chlorite) ratio and sea-level variations (Fig. 7a) are insignificant. In contrast, the Indian summer monsoon wind strength demonstrates strong 41-kyr and 23-kyr periodicities with a moderate one for 100 kyr (below 95% coherency, Fig. 6c). Meanwhile, the cross-spectral analysis suggests a strong correlation at 23-kyr periodicity but a moderate 100-kyr periodicity (Fig. 7b), implying a strong influence of the 23-kyr cycle from the Indian summer monsoon on the smectite/(illite+chlorite) ratio. Nevertheless, the dominant 100-kyr cycle in the smectite/(illite+chlorite) ratio claims a leading role with respect to sea-level variation in determining sediment transport from the Deccan Traps and Indus River to IODP Site U1457 over the past 600 kyr.

### **5.3 Dynamics of sediment transfer the eastern Arabian Sea: turbidite activity**

Turbidite activity is an important way for sediment transport from estuary to the deep sea (Bourget et al., 2010; Prins et al., 2000b). Turbidite deposits are mainly sourced from the Indus River, as supported by somewhat lower  $\epsilon\text{Nd}$  values (-13.7 to -13) compared with those of hemipelagic deposits (-12.7 to -9.4) (Fig. 4). Mishra et al. (2016) have recently identified the modern deep-sea channel systems within the Laxmi basin using high-resolution multibeam bathymetric data. We replot these newly recognized deep-sea channel systems together with the location of IODP Site U1457 in Figure 78. According to this study, IODP Site U1457 is located very close to one deep-sea channel system (Fig. 8) that may connect to the Indus River and bring large amounts of Indus sediment during the glacial periods (Mishra et al., 2016). Although the actual position of the deep-sea channel system may migrate widely through time, this study indicates strong turbidite activity in the Laxmi basin which could play an important role in the sediment transportation. Turbidite deposits every 2 kyr at IODP Site U1457 (Fig. 5c) are identified by combined visual description and XRF data (unpublished data from Mitchell Lyle). The turbidite layers in the studied area are mainly composed of heavy minerals which are generally rich in Ca and Zr but are barren in Al (Mange and Morton, 2007; Morton, 1991). Therefore, turbidity layers are associated with high heavy mineral proportions and increased Zr/Al or Ca/Al ratios. Besides, the appearance of turbidite layers in the core image is strongly contrasting with the hemipelagic deposit and could be easily identified by visual inspection. Generally, the higher turbidite frequency in IODP Site U1457 occurs during

glacial periods and cold substages of the interglacial periods (sea-level lowstands), and lower ones, on the contrary, occur during the warm interglacial periods (sea-level highstands). Such glacial–interglacial variations in the turbidite frequency could be due to seaward migration of the Indus River and reconnection between the river mouth and the head of deep-sea channels during the sea-level lowstands. Alternatively, these turbidites may rework deep-sea sediments located in a more northerly position and consequently characterized by a higher proportion of Indus River sediments (transported previously by oceanic currents). Therefore, the turbidite deposits at IODP Site U1457 imprint an important record of middle Indus Fan evolution in the eastern Arabian Sea since 600 kyr, as most of the previous sedimentological studies have focused on the upper and west Indus Fan channel system (Bourget et al., 2010; Prins et al., 2000b). Hemipelagic sediments of the glacial period could also be transported by turbidite currents and correspond to very distal sedimentation of turbidites (retransported by the currents). Nevertheless, our results here indicate that sea-level lowstands could reactivate north-south deep-sea channels of the Laxmi basin and permit transportation of sediments southward from the Indus River.

## **6. Conclusions**

Clay mineralogy and Sr-Nd isotopic compositions of the detrital fraction of sediments from IODP Site U1457 (Laxmi basin) have been analyzed to identify the sediment sources and establish the evolution of sediment dynamics for the eastern Arabian Sea since the last 600 kyr. The clay mineralogy and Sr-Nd isotopic compositions show that the detrital fraction at IODP Site U1457 results mainly from the mixing of sediment from the Deccan Traps and the Indus River and excludes a significant contribution of eolian dust to the Laxmi Basin. The smectite/(illite+chlorite) ratio in sediments taken from IODP Site U1457 was used to reconstruct the balance of sediment transport from the Indus River (mainly illite, chlorite and kaolinite) and from the Deccan Traps (smectite). This mineralogical ratio was higher and more variable during interglacial than glacial MIS. Wavelet and cross-spectral analyses reveal that sea-level variation (fluctuating mainly at 100 kyr) is the first-order controlling factor that has influenced sediment transport to the eastern Arabian Sea over the past 600 kyr. The Indian summer monsoon might contribute a moderate part of the variation, in particular in the precession (23-kyr) band. Compared with the hemipelagic deposits, the turbidite layers are generally associated with more unradiogenic  $\epsilon\text{Nd}$ . Such compositions suggest a higher relative proportion of Indus River sediments for these turbidite deposits. More Indus River sediment inputs to IODP Site U1457 during sea-level lowstands is probably due to a reconnection between the river mouth and the head of deep-sea channels and/or the reworking of Indus River-sourced sediments located in a more northerly position.



## Acknowledgments

The original data of this study is available in supporting information Table S1. We especially thank Louise Bordier and Arnaud Dapoigny for their assistance with Sr and Nd isotopic composition measurements. We wish to thank the scientific party and crew of the JOIDES Resolution for coring the samples in the Arabian Sea (International Ocean Discovery Program Expedition 355). Z. Yu acknowledges the China Scholarship Council (201304910385) for providing funding for his overseas study. The authors also thank Prof. A. Mackensen and the staff of the Alfred Wegener Institute for Polar and Marine Research, Germany, for the stable oxygen isotopic analysis of planktonic foraminifera. RS acknowledges the financial support from the Director, National Institute of Oceanography, Goa, India, IODP India and the Ministry of Earth Sciences, Government of India. This research used samples and/or data provided by the International Ocean Discovery Program (IODP). Funding for this research was provided by the Labex L596 IPSL (n°ANR-10-LABX-0018) and by IODP France.

## Reference

- Alagarsamy, R., Zhang, J., 2005. Comparative studies on trace metal geochemistry in Indian and Chinese rivers. *Current Science* 89, 299-309.
- Alizai, A., Hillier, S., Clift, P.D., Giosan, L., Hurst, A., VanLaningham, S., Macklin, M., 2012. Clay mineral variations in Holocene terrestrial sediments from the Indus Basin. *Quaternary Research* 77, 368-381.
- An, Z., Clemens, S.C., Shen, J., Qiang, X., Jin, Z., Sun, Y., Prell, W.L., Luo, J., Wang, S., Xu, H., 2011. Glacial-interglacial Indian summer monsoon dynamics. *science* 333, 719-723.
- An, Z., Kutzbach, J.E., Prell, W.L., Porter, S.C., 2001. Evolution of Asian monsoons and phased uplift of the Himalaya–Tibetan plateau since Late Miocene times. *Nature* 411, 62-66.
- Babechuk, M.G., Widdowson, M., Kamber, B.S., 2014. Quantifying chemical weathering intensity and trace element release from two contrasting basalt profiles, Deccan Traps, India. *Chemical Geology* 363, 56-75.
- Beal, L.M., Hormann, V., Lumpkin, R., Foltz, G.R., 2014. The Response of the Surface Circulation of the Arabian Sea to Monsoonal Forcing. *Journal of Physical Oceanography* 43, 2008-2022.
- Bernhardt, A., Schwanghart, W., Hebbeln, D., Stuut, J.-B.W., Strecker, M.R., 2017. Immediate propagation of deglacial environmental change to deep-marine turbidite systems along the Chile convergent margin. *Earth and Planetary Science Letters* 473, 190-204.
- Bhattacharyya, T., Pal, D., Deshpande, S., 1993. Genesis and transformation of minerals in the formation of red (Alfisols) and black (Inceptisols and Vertisols) soils on Deccan basalt in the Western Ghats, India. *Journal of Soil Science* 44, 159-171.

- Bintanja, R., Wal, R.S.W.V.D., Oerlemans, J., 2005. Modelled atmospheric temperatures and global sea levels over the past million years. *Nature* 437, 125.
- Biscaye, P.E., 1965. Mineralogy and sedimentation of recent deep-sea clay in the Atlantic Ocean and adjacent seas and oceans. *Geological Society of America Bulletin* 76, 803-832.
- Bourget, J., Zaragosi, S., Ellouz-Zimmermann, S., Ducassou, E., Prins, M.A., Garlan, T., Lanfume, V., Schneider, J.L., Rouillard, P., Giraudeau, J., 2010. Highstand vs. lowstand turbidite system growth in the Makran active margin: Imprints of high-frequency external controls on sediment delivery mechanisms to deep water systems. *Marine Geology* 274, 187-208.
- Bourget, J., Zaragosi, S., Rodriguez, M., Fournier, M., Garlan, T., Chamot-Rooke, N., 2013. Late Quaternary megaturbidites of the Indus Fan: Origin and stratigraphic significance. *Marine Geology* 336, 10-23.
- Caley, T., Malaizé, B., Zaragosi, S., Rossignol, L., Bourget, J., Eynaud, F., Martinez, P., Giraudeau, J., Charlier, K., Ellouz-Zimmermann, N., 2011. New Arabian Sea records help decipher orbital timing of Indo-Asian monsoon. *Earth and Planetary Science Letters* 308, 433-444.
- Castelltort, S., Van Den Driessche, J., 2003. How plausible are high-frequency sediment supply-driven cycles in the stratigraphic record? *Sedimentary Geology* 157, 3-13.
- Chamley, H., 1989. *Clay sedimentology*. Berlin: Springer.
- Clemens, S.C., Murray, D.W., Prell, W.L., 1996. Nonstationary Phase of the Plio-Pleistocene Asian Monsoon. *Science* 274, 943.
- Clemens, S.C., Prell, W.L., 1990. Late Pleistocene variability of Arabian Sea summer monsoon winds and continental aridity: Eolian records from the lithogenic component of deep-sea sediments. *Paleoceanography* 5, 109-145.
- Clemens, S.C., Prell, W.L., 2003. A 350,000 year summer-monsoon multi-proxy stack from the Owen Ridge, Northern Arabian Sea. *Marine Geology* 201, 35-51.
- Clift, Giosan, L., Carter, A., Garzanti, E., Galy, V., Tabrez, A.R., Pringle, M., Campbell, I.H., Francelanord, C., Blusztajn, J., 2010. Monsoon control over erosion patterns in the Western Himalaya: possible feed-back into the tectonic evolution. *Geological Society London Special Publications* 342.
- Clift, P., Shimizu, N., Layne, G., Blusztajn, J., Gaedicke, C., Schlüter, H.-U., Clark, M., Amjad, S., 2001. Development of the Indus Fan and its significance for the erosional history of the Western Himalaya and Karakoram. *Geological Society of America Bulletin* 113, 1039-1051.
- Clift, P.D., Giosan, L., Blusztajn, J., Campbell, I.H., Allen, C., Pringle, M., Tabrez, A.R., Danish, M., Rabbani, M.M., Alizai, A., 2008. Holocene erosion of the Lesser Himalaya triggered by intensified summer monsoon. *Geology* 36, 79-82.

- Colin, C., Siani, G., Sicre, M.-A., Liu, Z., 2010. Impact of the East Asian monsoon rainfall changes on the erosion of the Mekong River basin over the past 25,000 yr. *Marine Geology* 711 271, 84-92.
- Colin, C., Turpin, L., Bertaux, J., Desprairies, A., Kissel, C., 1999. Erosional history of the Himalayan and Burman ranges during the last two glacial–interglacial cycles. *Earth and Planetary Science Letters* 171, 647-660.
- Colin, C., Turpin, L., Blamart, D., Frank, N., Kissel, C., Duchamp, S., 2006. Evolution of weathering patterns in the Indo-Burman Ranges over the last 280 kyr: Effects of sediment provenance on  $^{87}\text{Sr}/^{86}\text{Sr}$  ratios tracer. *Geochemistry, Geophysics, Geosystems* 7.
- Copard, K., Colin, C., Douville, E., Freiwald, A., Gudmundsson, G., De Mol, B., Frank, N., 2010. Nd isotopes in deep-sea corals in the North-eastern Atlantic. *Quaternary Science Reviews* 29, 2499-2508.
- Das, A., Krishnaswami, S., Sarin, M., Pande, K., 2005. Chemical weathering in the Krishna Basin and Western Ghats of the Deccan Traps, India: rates of basalt weathering and their controls. *Geochimica et Cosmochimica Acta* 69, 2067-2084.
- Dessert, C., Dupré, B., François, L.M., Schott, J., Gaillardet, J., Chakrapani, G., Bajpai, S., 2001. Erosion of Deccan Traps determined by river geochemistry: impact on the global climate and the  $^{87}\text{Sr}/^{86}\text{Sr}$  ratio of seawater. *Earth and Planetary Science Letters* 188, 459-474.
- Ehrmann, W., 1998. Implications of late Eocene to early Miocene clay mineral assemblages in McMurdo Sound (Ross Sea, Antarctica) on paleoclimate and ice dynamics. *Palaeogeography, Palaeoclimatology, Palaeoecology* 139, 213-231.
- Esquevin, J., 1969. Influence de la composition chimique des illites sur leur cristallinité. *Bull. Centre Rech. Pau-SNPA* 3, 147-153.
- Fournier, L., Fauquembergue, K., Zaragosi, S., Zorzi, C., Malaize, B., Bassinot, F., Joussain, R., Colin, C., Moreno, E., Leparmentier, F., 2017. The Bengal fan: External controls on the Holocene Active Channel turbidite activity. *Holocene* 27, 900-913.
- Galy, A., France-Lanord, C., 2001. Higher erosion rates in the Himalaya: geochemical constraints on riverine fluxes. *Geology* 29, 23-26.
- Gao, S., Collins, M.B., 2014. Holocene sedimentary systems on continental shelves. *Marine Geology* 352, 268-294.
- Goswami, V., Singh, S.K., Bhushan, R., Rai, V.K., 2012. Temporal variations in  $^{87}\text{Sr}/^{86}\text{Sr}$  and  $\epsilon\text{Nd}$  in sediments of the southeastern Arabian Sea: Impact of monsoon and surface water circulation. *Geochemistry, Geophysics, Geosystems* 13.
- Grousset, F.E., Biscaye, P.E., 2005. Tracing dust sources and transport patterns using Sr, Nd and Pb isotopes. *Chemical Geology* 222, 149-167.
- Haq, B.U., Milliman, J.D., 1984. Marine geology and oceanography of Arabian Sea and coastal Pakistan. Unknown.

- Heller, F., Liu, T.S., 1982. Magnetostratigraphical dating of loess deposits in China. *Nature* 300, 431-433.
- Howe, J.N., Piotrowski, A.M., Noble, T.L., Mulitza, S., Chiessi, C.M., Bayon, G., 2016. North Atlantic Deep Water Production during the Last Glacial Maximum. *Nature Communications* 7, 11765.
- Jacobsen, S.B., Wasserburg, G., 1980. Sm-Nd isotopic evolution of chondrites. *Earth and Planetary Science Letters* 50, 139-155.
- Joussain, R., Colin, C., Liu, Z.F., Meynadier, L., Fournier, L., Fauquembergue, K., Zaragosi, S., Schmidt, F., Rojas, V., Bassinot, F., 2016. Climatic control of sediment transport from the Himalayas to the proximal NE Bengal Fan during the last glacial-interglacial cycle. *Quaternary Science Reviews* 148, 1-16.
- Joussain, R., Liu, Z.F., Colin, C., Duchamp-Alphonse, S., Yu, Z.J., Moreno, E., Fournier, L., Zaragosi, S., Dapoigny, A., Meynadier, L., Bassinot, F., 2017. Link between Indian monsoon rainfall and physical erosion in the Himalayan system during the Holocene. *Geochem Geophys Geosy* 18, 3452-3469.
- Keller, G., Adatte, T., Bajpai, S., Mohabey, D., Widdowson, M., Khosla, A., Sharma, R., Khosla, S., Gertsch, B., Fleitmann, D., 2009. K–T transition in Deccan Traps of central India marks major marine Seaway across India. *Earth and Planetary Science Letters* 282, 10-23.
- Kessarkar, P.M., Rao, V.P., Ahmad, S., Babu, G.A., 2003. Clay minerals and Sr–Nd isotopes of the sediments along the western margin of India and their implication for sediment provenance. *Marine Geology* 202, 55-69.
- King, J.W., Channell, J.E.T., 1991. SEDIMENTARY MAGNETISM, ENVIRONMENTAL MAGNETISM, AND MAGNETOSTRATIGRAPHY. *Reviews of Geophysics* 29, 358-370.
- Kolla, V., Kostecki, J., Robinson, F., Biscaye, P., Ray, P., 1981. Distributions and origins of clay minerals and quartz in surface sediments of the Arabian Sea. *Journal of Sedimentary Research* 51.
- Kripalani, R., Kulkarni, A., 2001. Monsoon rainfall variations and teleconnections over South and East Asia. *International Journal of Climatology* 21, 603-616.
- Laskar, J., Robutel, P., Joutel, F., Gastineau, M., Correia, A., Levrard, B., 2004. A long-term numerical solution for the insolation quantities of the Earth. *Astronomy & Astrophysics* 428, 261-285.
- Li, G., Li, P., Liu, Y., Qiao, L., Ma, Y., Xu, J., Yang, Z., 2014. Sedimentary system response to the global sea level change in the East China Seas since the last glacial maximum. *Earth-Science Reviews* 139, 390-405.
- Lightfoot, P., Hawkesworth, C., 1988. Origin of Deccan Trap lavas: evidence from combined trace element and Sr-, Nd- and Pb-isotope studies. *Earth & Planetary Science Letters* 91, 89- 104.
- Limmer, D.R., Böning, P., Giosan, L., Ponton, C., Köhler, C.M., Cooper, M.J., Tabrez, A.R., Clift, P.D., 2012. Geochemical record of Holocene to Recent sedimentation on the Western Indus continental shelf, Arabian Sea. *Geochemistry, Geophysics, Geosystems* 13.

- Lisiecki, L., Raymo, M., 2005. A Pliocene-Pleistocene stack of 57 globally distributed benthic  $\delta^{18}\text{O}$  records. *Paleoceanography* 20, PA1003.
- Liu, Z., Colin, C., Trentesaux, A., Blamart, D., Bassinot, F., Siani, G., Sicre, M.-A., 2004. Erosional history of the eastern Tibetan Plateau since 190 kyr ago: clay mineralogical and geochemical investigations from the southwestern South China Sea. *Marine Geology* 209, 1-18.
- Liu, Z., Trentesaux, A., Clemens, S.C., Colin, C., Wang, P., Huang, B., Boulay, S., 2003. Clay mineral assemblages in the northern South China Sea: implications for East Asian monsoon evolution over the past 2 million years. *Marine Geology* 201, 133-146.
- Liu, Z., Zhao, Y., Colin, C., Stattegger, K., Wiesner, M.G., Huh, C.-A., Zhang, Y., Li, X., Sompongchaiyakul, P., You, C.-F., 2015. Source-to-Sink transport processes of fluvial sediments in the South China Sea. *Earth-Science Reviews* 153, 238-273.
- Lugmair, G., Shimamura, T., Lewis, R., Anders, E., 1983. Samarium-146 in the early solar system: evidence from neodymium in the Allende meteorite. *science* 222, 1015-1018.
- Mackenzie, R., Wilson, M., Mashhady, A., 1984. Origin of palygorskite in some soils of the Arabian Peninsula. *Developments in Sedimentology* 37, 177-186.
- Mange, M.A., Morton, A.C., 2007. Geochemistry of heavy minerals. *Developments in sedimentology* 58, 345-391.
- McHargue, T.R., Webb, J.E., 1986. Internal geometry, seismic facies, and petroleum potential of canyons and inner fan channels of the Indus submarine fan. *AAPG Bulletin* 70, 161-180.
- Milliman, J.D., Meade, R.H., 1983. World-wide delivery of river sediment to the oceans. *The Journal of Geology*, 1-21.
- Mishra, R., Pandey, D.K., Ramesh, P., Clift, P.D., 2016. Identification of new deep sea sinuous channels in the eastern Arabian Sea. *Springerplus* 5, 1-18.
- Morton, A.C., 1991. Geochemical studies of detrital heavy minerals and their application to provenance research. *Geological Society, London, Special Publications* 57, 31-45.
- Pandey, D., Clift, P., Kulhanek, D., Andò, S., Bendle, J., Bratenkov, S., Griffith, E., Gurumurthy, G., Hahn, A., Iwai, M., Khim, B.-K., Kumar, A., Kumar, A.G., Liddy, H.M., Lu, H., Lyle, M.W., Mishra, R., Radhakrishna, T., Routledge, C.M., Saraswat, R., Saxena, R., Scardia, G., Sharma, G.K., Singh, A.D., Steinke, S., Suzuki, K., Tauxe, L., Tiwari, M., Xu, Z., Yu, Z., 2015. Expedition 355 Preliminary Report: Arabian Sea Monsoon. *International Ocean Discovery Program*. <http://dx.doi.org/10.14379/iodp.pr.355.2015>.
- Peizhen, Z., Molnar, P., Downs, W.R., 2001. Increased sedimentation rates and grain sizes 2–4 Myr ago due to the influence of climate change on erosion rates. *Nature* 410, 891-897.
- Petschick, R., Kuhn, G., Gingele, F., 1996. Clay mineral distribution in surface sediments of the South Atlantic: sources, transport, and relation to oceanography. *Marine Geology* 130, 203-229.

- Phillips, S.C., Johnson, J.E., Underwood, M.B., Guo, J., Giosan, L., Rose, K., 2014. Long-timescale variation in bulk and clay mineral composition of Indian continental margin sediments in the Bay of Bengal, Arabian Sea, and Andaman Sea. *Marine & Petroleum Geology* 58, 117-138.
- Piotrowski, A.M., Banakar, V.K., Scrivner, A.E., Elderfield, H., Galy, A., Dennis, A., 2009. Indian Ocean circulation and productivity during the last glacial cycle. *Earth and Planetary Science Letters* 285, 179-189.
- Posamentier, H.W., Vail, P.R., 1988. Eustatic controls on clastic deposition II – Sequence and Systems Tract Models.
- Pourmand, A., Marcantonio, F., Schulz, H., 2004. Variations in productivity and eolian fluxes in the northeastern Arabian Sea during the past 110 ka. *Earth and Planetary Science Letters* 221, 39-54.
- Prins, M., Postma, G., Cleveringa, J., Cramp, A., Kenyon, N., 2000a. Controls on terrigenous sediment supply to the Arabian Sea during the late Quaternary: the Indus Fan. *Marine Geology* 169, 327-349.
- Prins, M., Postma, G., Weltje, G.J., 2000b. Controls on terrigenous sediment supply to the Arabian Sea during the late Quaternary: the Makran continental slope. *Marine Geology* 169, 351-371.
- Prins, M.A., Postma, G., 2000. Effects of climate, sea level, and tectonics unraveled for last deglaciation turbidite records of the Arabian Sea. *Geology* 28, 375-378.
- Prins, M.A., Weltje, G.J., 1999. End-member modeling of siliciclastic grain-size distributions: the late Quaternary record of eolian and fluvial sediment supply to the Arabian Sea and its paleoclimatic significance.
- Ramaswamy, V., Nair, R.R., 1994. Fluxes of material in the Arabian Sea and Bay of Bengal - Sediment trap studies. *Proceedings of the Indian Academy of Sciences - Earth and Planetary Sciences* 103, 189-210.
- Rao, V.P., Rao, B.R., 1995. Provenance and distribution of clay minerals in the sediments of the western continental shelf and slope of India. *Continental Shelf Research* 15, 1757-1771.
- Sarin, M., Krishnaswami, S., Dilli, K., Somayajulu, B., Moore, W., 1989. Major ion chemistry of the Ganga-Brahmaputra river system: Weathering processes and fluxes to the Bay of Bengal. *Geochimica et cosmochimica acta* 53, 997-1009.
- Scheuvens, D., Schütz, L., Kandler, K., Ebert, M., Weinbruch, S., 2013. Bulk composition of northern African dust and its source sediments — A compilation. *Earth-science Reviews* 116, 170-194.
- Shadfan, H., Mashhady, A., 1985. Distribution of palygorskite in sediments and soils of eastern Saudi Arabia. *Soil Science Society of America Journal* 49, 243-250.
- Shetye, S., Gouveia, A., Shenoi, S., 1994. Circulation and water masses of the Arabian Sea. *Proceedings of the Indian Academy of Sciences-Earth and Planetary Sciences* 103, 107-123.
- Singh, R.N., Gupta, K.R., 2013. Workshop yields new insight into volcanism at Deccan Traps, India. *Eos Transactions American Geophysical Union* 75, 356-356.

- Sirocko, F., Lange, H., 1991. Clay-mineral accumulation rates in the Arabian Sea during the late Quaternary. *Marine Geology* 97, 105-119.
- Sirocko, F., Sarnthein, M., 1989. Wind-Borne Deposits in the Northwestern Indian Ocean: Record of Holocene Sediments Versus Modern Satellite Data. Springer Netherlands.
- Stein, M., Goldstein, S.L., 1996. From plume head to continental lithosphere in the Arabian–Nubian shield. *Nature* 382, 773-778.
- Steinke, S., Chiu, H.Y., Yu, P.S., Shen, C.C., Erlenkeuser, H., Löwemark, L., Chen, M.T., 2006. On the influence of sea level and monsoon climate on the southern South China Sea freshwater budget over the last 22,000 years. *Quaternary Science Reviews* 25, 1475-1488.
- Steinke, S., Hanebuth, T.J., Vogt, C., Stattegger, K., 2008. Sea level induced variations in clay mineral composition in the southwestern South China Sea over the past 17,000 yr. *Marine Geology* 250, 199-210.
- Steinke, S., Kienast, M., Hanebuth, T., 2003. On the significance of sea-level variations and shelf paleo-morphology in governing sedimentation in the southern South China Sea during the last deglaciation. *Marine Geology* 201, 179-206.
- Stoeser, D.B., Frost, C.D., 2006. Nd, Pb, Sr, and O isotopic characterization of Saudi Arabian Shield terranes. *Chemical Geology* 226, 163-188.
- Tanaka, T., Togashi, S., Kamioka, H., Amakawa, H., Kagami, H., Hamamoto, T., Yuhara, M., Orihashi, Y., Yoneda, S., Shimizu, H., 2000. JNdi-1: a neodymium isotopic reference in consistency with LaJolla neodymium. *Chemical Geology* 168, 279-281.
- Tateo, F., Sabbadini, R., Morandi, N., 2000. Palygorskite and sepiolite occurrence in Pliocene lake deposits along the River Nile: evidence of an arid climate. *Journal of African Earth Sciences* 31, 633-645.
- Torrence, C., Compo, G.P., 1998. A practical guide to wavelet analysis. *Bulletin of the American Meteorological society* 79, 61-78.
- Unger, D., Ittekkot, V., Schäfer, P., Tiemann, J., Reschke, S., 2003. Seasonality and interannual variability of particle fluxes to the deep Bay of Bengal: influence of riverine input and oceanographic processes. *Deep Sea Research Part II: Topical Studies in Oceanography* 50, 897-923.
- Verrecchia, Coustumer, 1996a. Occurrence and Genesis of Palygorskite and Associated Clay Minerals in a Pleistocene Calcrete Complex, Sde Boqer, Negev Desert, Israel. *Clay Minerals* 31, 183-202.
- Verrecchia, E., Coustumer, M., 1996b. Occurrence and genesis of palygorskite and associated clay minerals in a Pleistocene calcrete complex, Sde Boqer, Negev Desert, Israel. *Clay Minerals* 31, 183-202.
- Wan, S., Clift, P.D., Zhao, D., Hovius, N., Munhoven, G., France-Lanord, C., Wang, Y., Xiong, Z., Huang, J., Yu, Z., Zhang, J., Ma, W., Zhang, G., Li, A., Li, T., 2017. Enhanced silicate weathering of tropical shelf sediments exposed during glacial lowstands: A sink for atmospheric CO<sub>2</sub>. *Geochimica et Cosmochimica Acta* 200, 123-144.

- Wan, S., Tian, J., Steinke, S., Li, A., Li, T., 2010. Evolution and variability of the East Asian summer monsoon during the Pliocene: Evidence from clay mineral records of the South China Sea. *Palaeogeography, Palaeoclimatology, Palaeoecology* 293, 237-247.
- Wan, S., Toucanne, S., Clift, P.D., Zhao, D., Bayon, G., Yu, Z., Cai, G., Yin, X., Révillon, S., Wang, D., 2015. Human impact overwhelms long-term climate control of weathering and erosion in southwest China. *Geology* 43, 439-442.
- Wan, S., Yu, Z., Clift, P.D., Sun, H., Li, A., Li, T., 2012. History of Asian eolian input to the West Philippine Sea over the last one million years. *Palaeogeography, Palaeoclimatology, Palaeoecology* 326, 152-159.
- Webster, P.J., 1987. The elementary monsoon. *Monsoons*, J. S. Fein and P. L. Stephens, eds., John Wiley and Sons, 3–32.
- West, A.J., Galy, A., Bickle, M., 2005. Tectonic and climatic controls on silicate weathering. *Earth and Planetary Science Letters* 235, 211-228.
- White, A.F., Blum, A.E., 1995. Effects of climate on chemical\_ weathering in watersheds. *Geochimica Et Cosmochimica Acta* 59, 1729-1747.
- Xu, Z., Li, T., Clift, P.D., Wan, S., Qiu, X., Lim, D., 2018. Bathyal records of enhanced silicate erosion and weathering on the exposed Luzon shelf during glacial lowstands and their significance for atmospheric CO<sub>2</sub> sink. *Chemical Geology* 476, 302-315.
- Yu, Z., Colin, C., Meynadier, L., Douville, E., Dapoigny, A., Reverdin, G., Wu, Q., Wan, S., Song, L., Xu, Z., 2017. Seasonal variations in dissolved neodymium isotope composition in the Bay of Bengal. *Earth and Planetary Science Letters* 479, 310-321.
- Yu, Z., Wan, S., Colin, C., Yan, H., Bonneau, L., Liu, Z., Song, L., Sun, H., Xu, Z., Jiang, X., 2016. Co-evolution of monsoonal precipitation in East Asia and the tropical Pacific ENSO system since 2.36 Ma: New insights from high-resolution clay mineral records in the West Philippine Sea. *Earth and Planetary Science Letters* 446, 45-55.



## Figure captions:

**Fig. 1** Bathymetric map showing the location of IODP Site U1457 as well as the nearby geologic structures (Arabian plate, Makran, Indo-Gangetic plain, Deccan Traps and Peninsular Gneisses) and marine sediment cores noted in this paper (cores ODP Site 722 (Clemens et al., 1996), Indus-10 (Limmer et al., 2012), Indus-23 (Limmer et al., 2012) and SS-3104G (Goswami et al., 2012)). Modern locations of the Indus Fan and Deccan Traps are indicated by the bold dashed lines. The surface circulations in the Arabian Sea in the summer (thick black line) and winter (thick white line) as well as the deep circulation (thick blue line) are also indicated, along with the major rivers. The mineralogical compositions of the clay-size fraction and Sr-Nd isotopic ratio of the main sedimentary sources as well as for core IODP Site U1457 are reported for comparison.

**Fig. 2.** Comparison of  $\delta^{18}\text{O}$  record from IODP Site U1457 (Saraswat et al., unpublished data) with the global benthic LR04 (Lisiecki and Raymo, 2005). The age-depth datum are marked with grey bands.

**Fig. 3** Variations in clay mineral assemblages, illite chemistry index and illite crystallinity at IODP Site U1457 since 600 kyr. The stacked global benthic  $\delta^{18}\text{O}$  record of LR04 (Lisiecki and Raymo, 2005) is shown for comparison. The shaded bars and numbers indicate interglacial marine isotope stages (MIS). Note that the black bar indicates the gap caused by the modification of composite depth after our sampling.

**Fig. 4** a) Correlation analysis of mean grain-size with  $\epsilon\text{Nd}$  from IODP Site U1457 (this study); b) Correlation analysis of mean grain-size with  $^{87}\text{Sr}/^{86}\text{Sr}$  from IODP Site U1457 (this study); c)  $^{87}\text{Sr}/^{86}\text{Sr}$  versus  $\epsilon\text{Nd}$  (0) of sediments from IODP Site U1457 (this study; note that the values from glacial and interglacial periods and turbidite layers are separated), together with sediments from cores SS-3104G (Goswami et al., 2012), Indus-10 NW Shelf and Indus-23 Clinoform (Limmer et al., 2012), rivers draining the Deccan Traps (Goswami et al., 2012; Lightfoot and Hawkesworth, 1988) and eolian dust from north Africa and central Arabia (Grousset and Biscaye, 2005; Scheuven et al., 2013); d) Ternary diagram showing variation in clay mineral compositions of sediments from IODP Site U1457 (this study) and sediments from rivers that drain the Deccan Traps (Kessarkar et al., 2003), Gneissic rock (Kessarkar et al., 2003) and the Indus River (Alizai et al., 2012; Kolla et al., 1981).

**Fig. 5** Comparison of a) smectite/(illite + chlorite) ratio (black line) and  $\epsilon\text{Nd}$  (red line) from IODP Site U1457 (this study); b) magnetic susceptibility variation from IODP Site U1457 (Pandey et al., 2015); c) turbidite frequency in core from IODP Site U1457 (this study); d) Indian summer monsoon wind strength reconstructed from lithogenic grain size of ODP Site 722 (Clemens et al., 1996) and

insolation at 30°N in June (Laskar et al., 2004); e) stacked global benthic  $\delta^{18}\text{O}$  record of LR04 (Lisiecki and Raymo, 2005) and global sea-level variation (Bintanja et al., 2005).

**Fig. 6** Wavelet power analysis for a) smectite/(illite + chlorite) ratio from IODP Site U1457 (this study); b) global sea-level variation (Bintanja et al., 2005); c) Indian summer monsoon wind strength reconstructed from lithogenic grain size of ODP Site 722 (Clemens et al., 1996). The solid black contour lines identify regions where spectral power meets the 5% significance level against red noise. Pale shading identifies the cone of influence where edge effects due to processing may impact upon the signal.

**Fig. 7** Cross-spectral relationships between the smectite/(illite + chlorite) ratio from IODP Site U1457 and a) global sea-level variation (Bintanja et al., 2005); b) Indian summer monsoon wind strength reconstructed from lithogenic grain size of ODP Site 722 (Clemens et al., 1996). Note that the spectral densities use log scales. The horizontal solid lines indicate confidence at the 80% and 95% levels.

**Fig. 8** Blocks A, B and C represent the locations of modern deep-sea channel systems within the Laxmi basin (Mishra et al., 2016). Note that IODP Site U1457 is located just south of the Block B system.

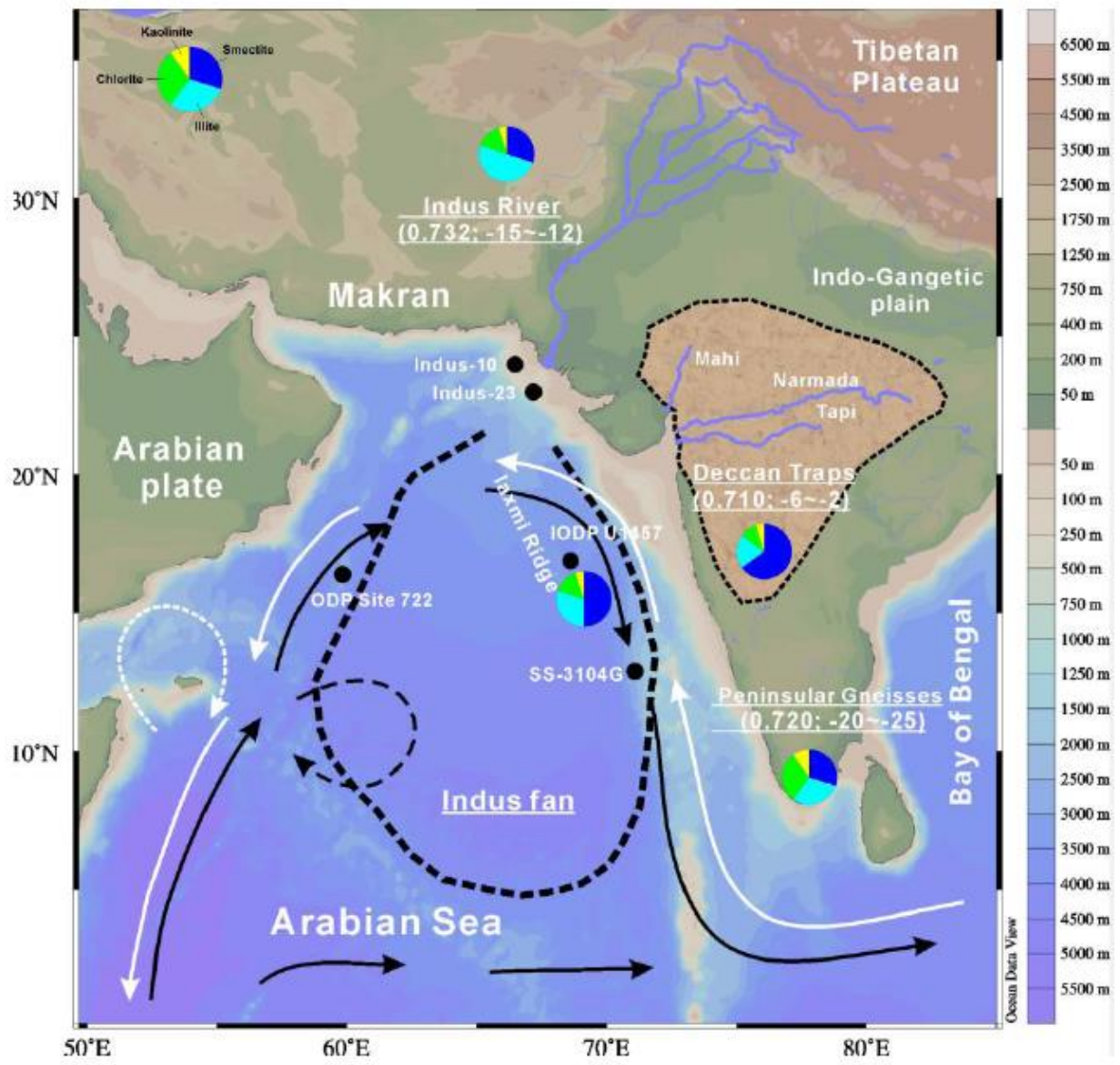
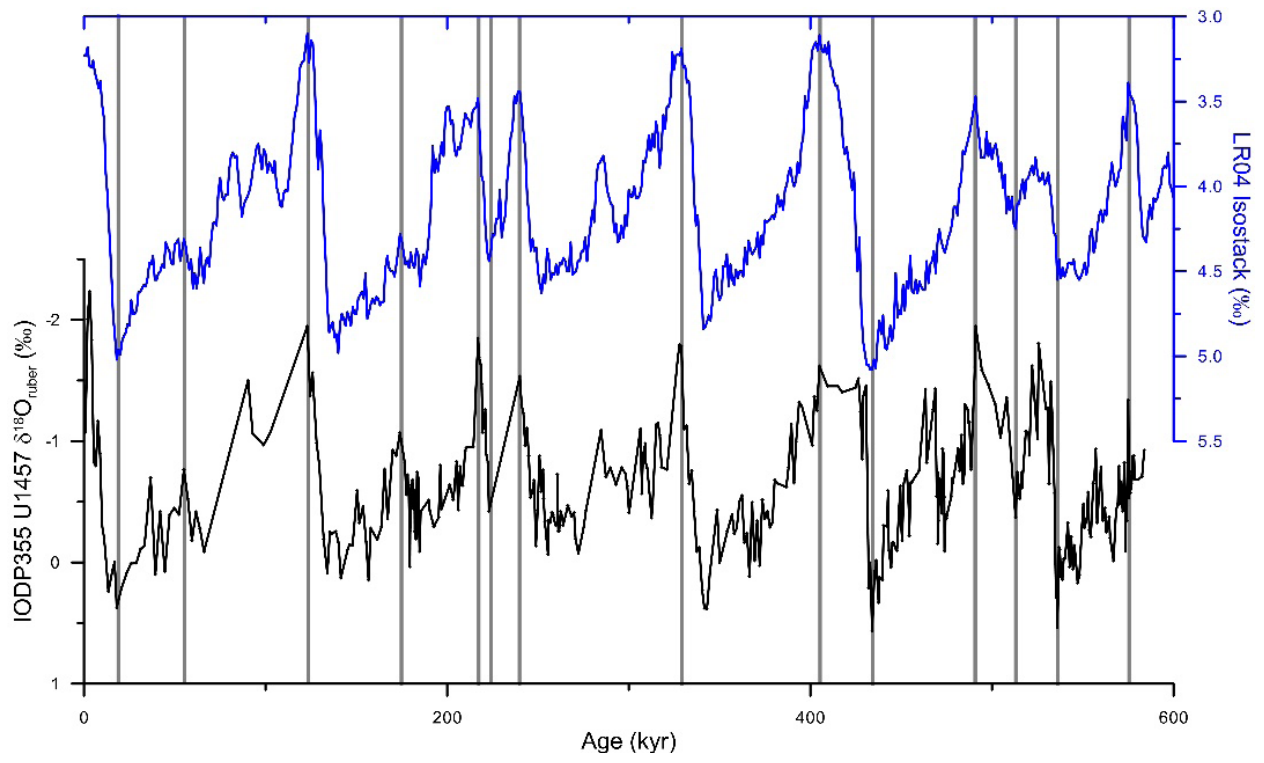


Figure 1



**Figure 2**

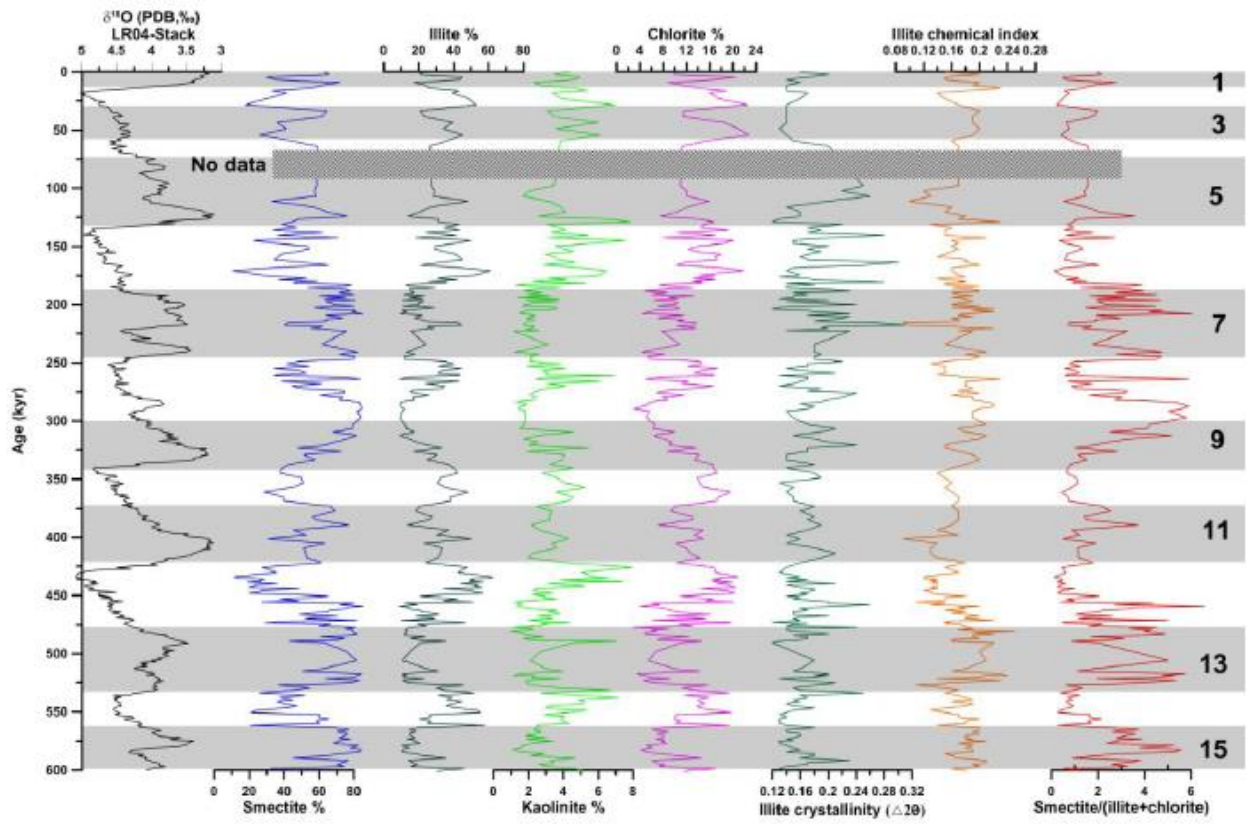


Figure 3

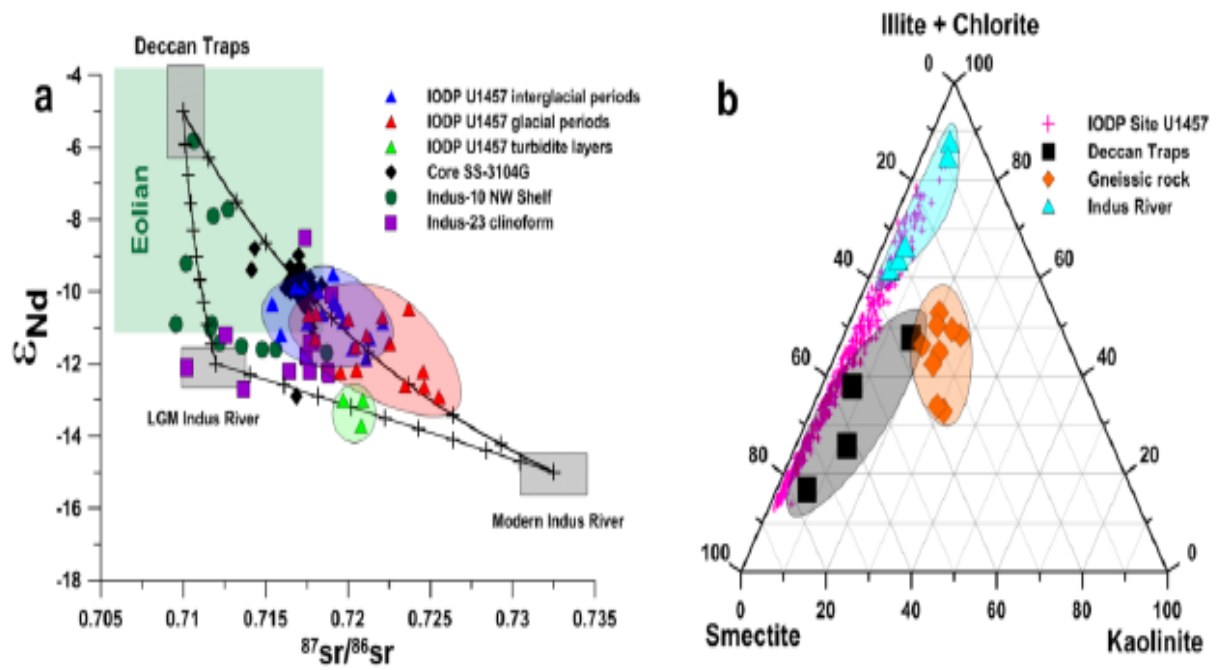


Figure 4

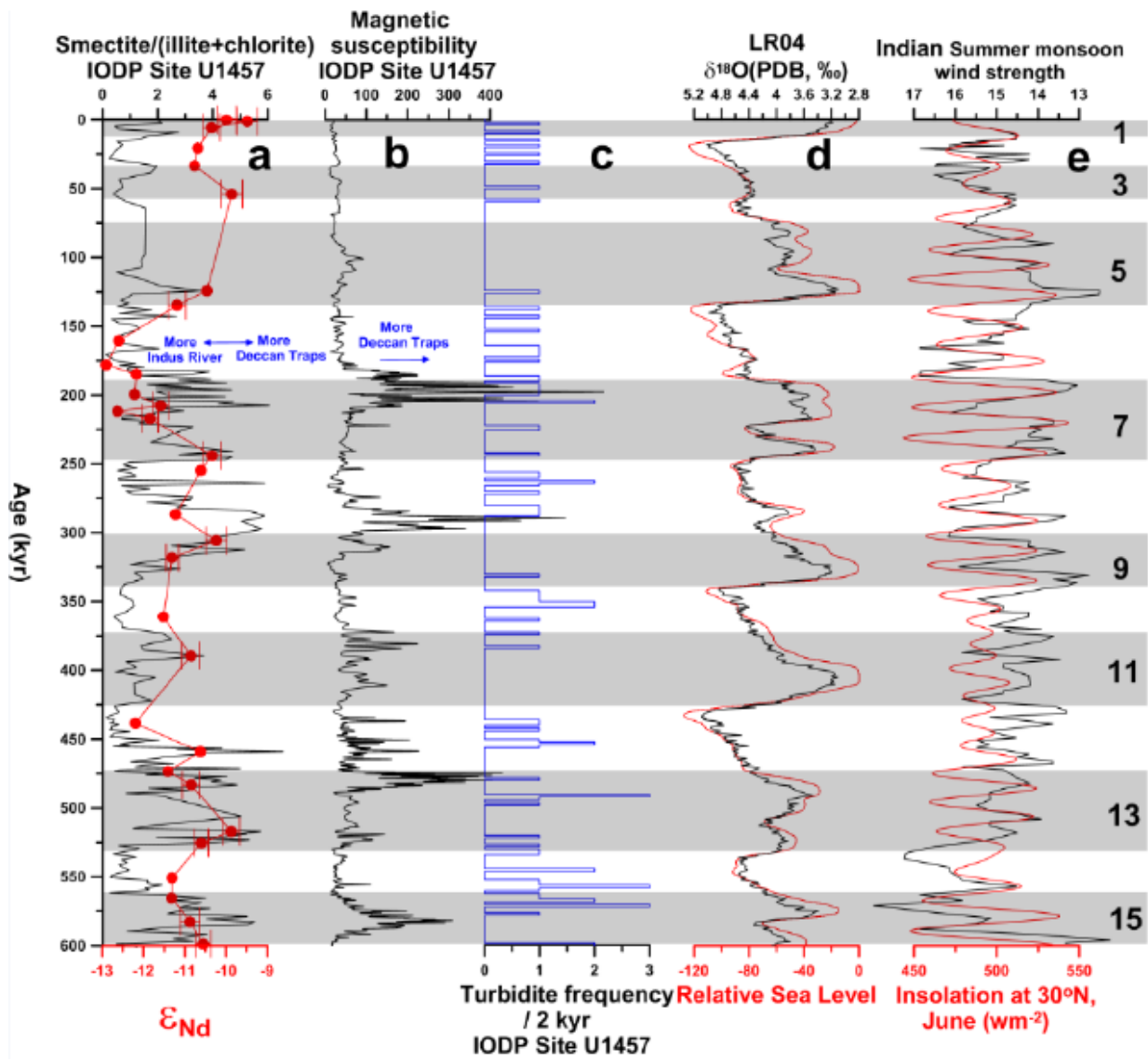


Figure 5

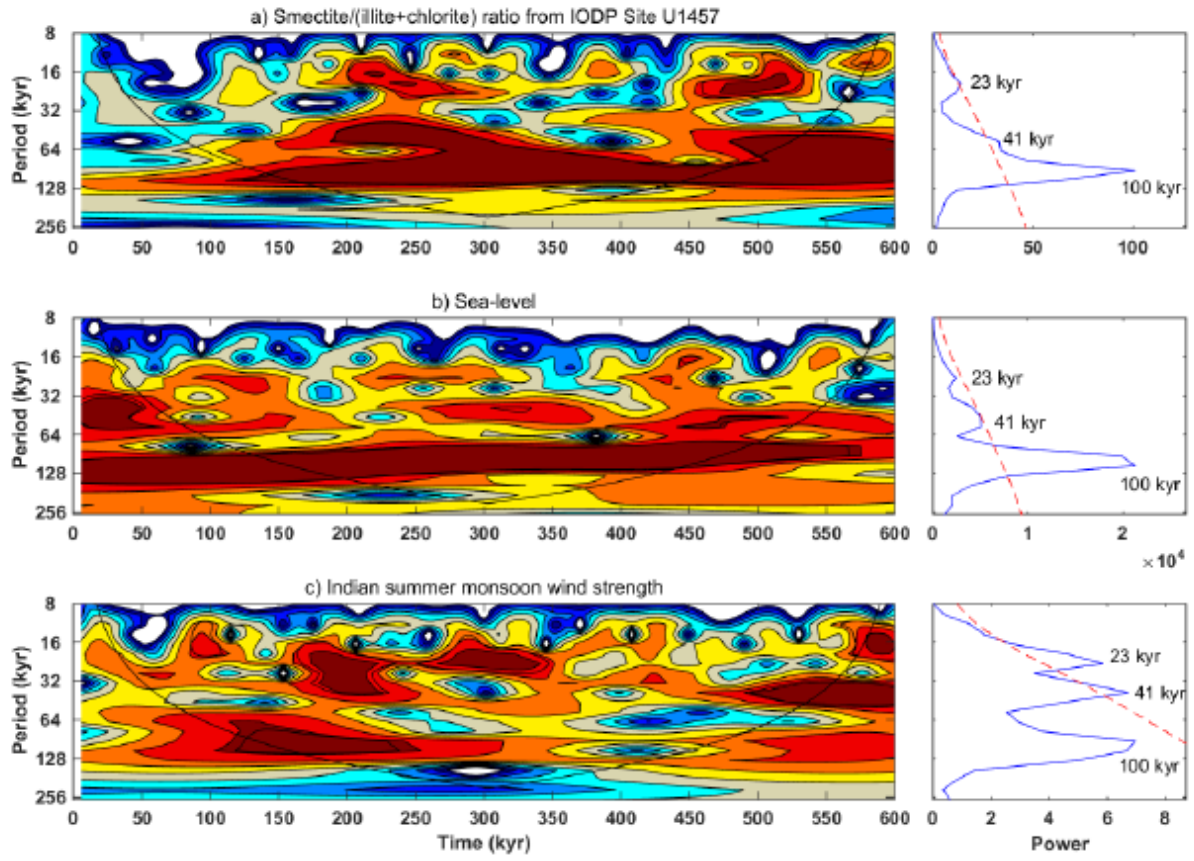
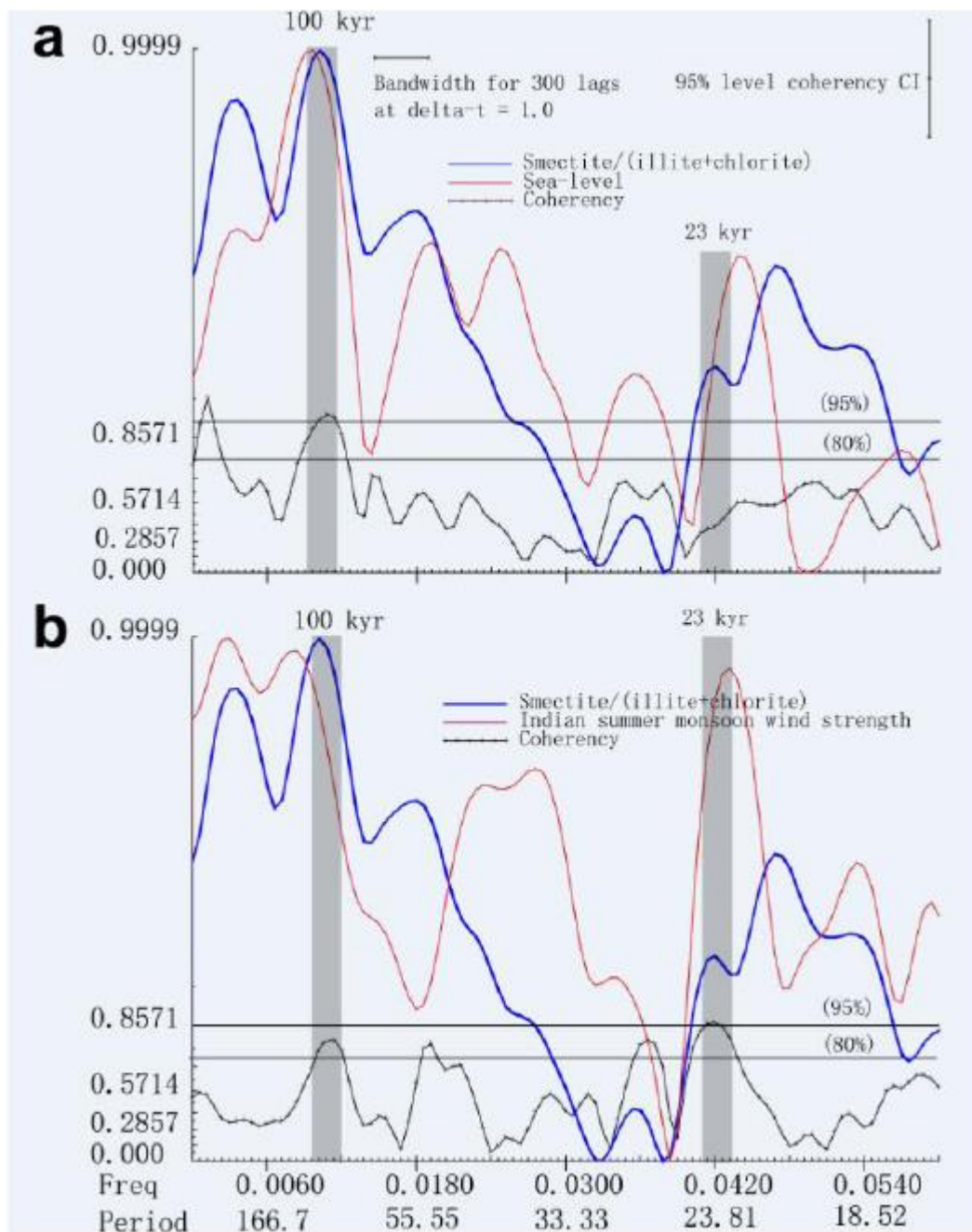


Figure 6





**Figure 7**

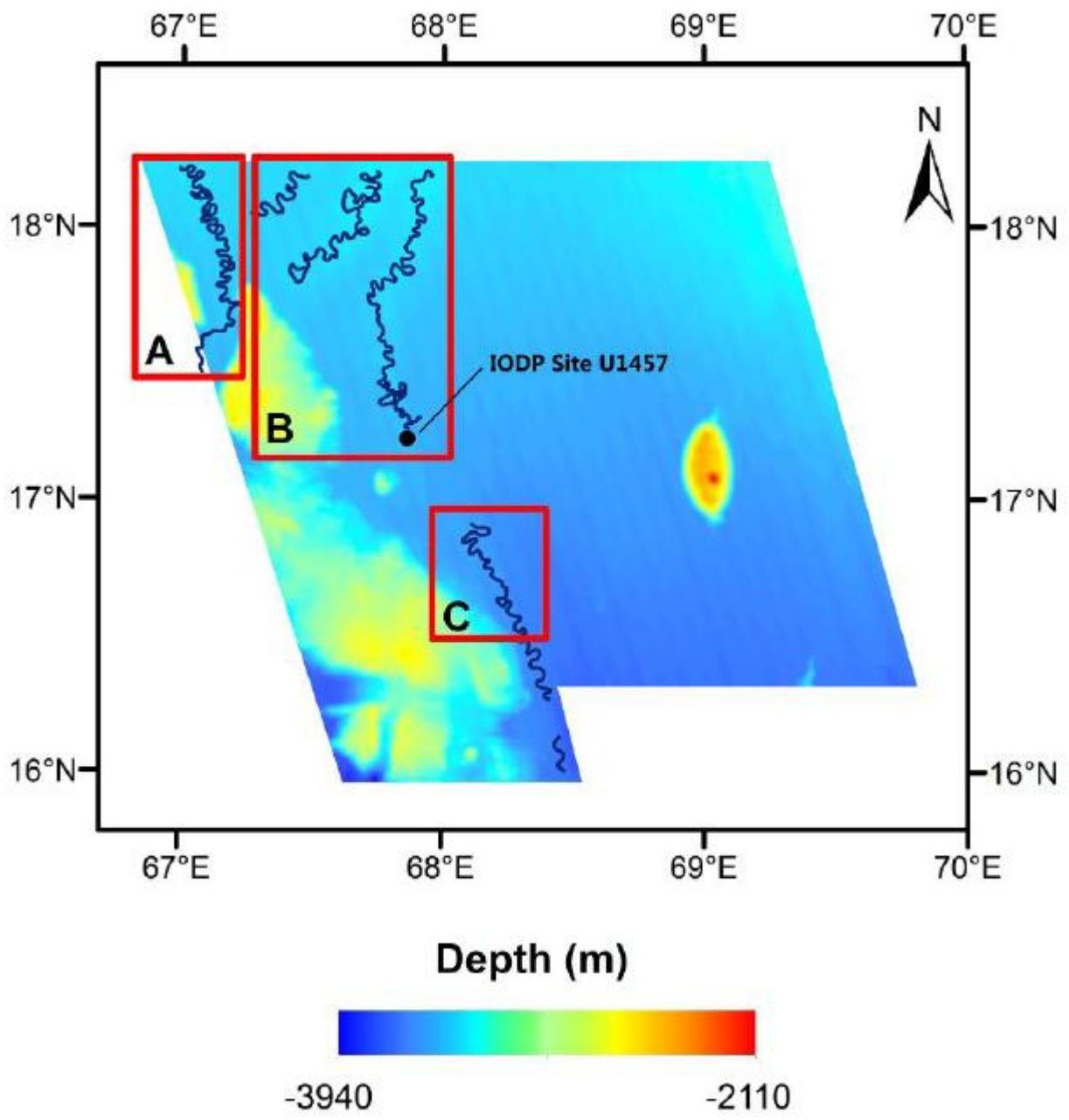


Figure 8

**Table 1** : Sample depths (cm) in core, type of deposits (T : turbidite layers, HP : hemipelagic layers), age of the sediments (kyr),  $^{87}\text{Sr}/^{86}\text{Sr}$ ,  $^{143}\text{Nd}/^{144}\text{Nd}$  and  $\epsilon\text{Nd}$  values, mean grain size as well as smectite (Smec), illite (Ill), chlorite (Chl) and kaolinite (kaol) proportions (%).  $\epsilon\text{Nd}$  was determined using the present CHUR value from Jacobsen and Wasserburg (1980),  $\epsilon\text{Nd}(0) = [(^{143}\text{Nd}/^{144}\text{Nd})_{\text{meas}}/0.512638 - 1] * 10000$ .

Core	Top depth CSF-A (m)	Bottom depth CSF-A (m)	Age (kyr)	Deposition	$^{87}\text{Sr}/^{86}\text{Sr}$	$\pm 2\sigma$	$^{143}\text{Nd}/^{144}\text{Nd}$	$\pm 2\sigma$	$\epsilon\text{Nd}$	$\pm 2\sigma$	Mean grain size ( $\mu\text{m}$ )	S%	I%	Ch %	K %
B1H1	0	0.02	0	HP	0.71818	1.43E-05	0.512128	1.16E-05	-10	0.2	9.6	63	23	10	4
B1H1	0.07	0.09	1	HP	0.71906	1.43E-05	0.512155	1.28E-05	-9.4	0.2	9.9	77	14	6	3
B1H1	0.35	0.37	6	HP	0.7192	1.43E-05	0.512118	1.02E-05	-10.1	0.2	18.4	22	53	20	5
B1H1	1.19	1.21	21	HP	0.72204	1.43E-05	0.512089	1.05E-05	-10.7	0.2	13.1	20	58	20	2
B1H2	1.54	1.56	33	HP	0.71998	1.43E-05	0.512084	1.17E-05	-10.8	0.2	11.6	64	21	12	3
B1H2	2.1	2.12	54	HP	0.71732	1.43E-05	0.512126	1.32E-05	-10	0.3	10.8	26	45	23	6
A1H2	1.08	1.1	124	HP	0.72364	1.43E-05	0.5121	1.12E-05	-10.5	0.2	9.6	76	14	8	3
A1H2	1.72	1.74	135	HP	0.71589	1.43E-05	0.512057	1.07E-05	-11.3	0.2	15.1	23	53	20	4
A1H3	3.26	3.28	160	HP	0.72343	1.43E-05	0.511988	8.77E-06	-12.7	0.2	13.9	28	51	18	3
A1H4	4.51	4.53	178	HP	0.72547	1.43E-05	0.511971	9.12E-06	-13	0.2	13.4	60	26	12	2
B2H1	4.58	4.6	185	HP	0.72047	1.43E-05	0.512019	9.87E-06	-12.1	0.2	9.9	79	12	7	2
B2H3	6.14	6.16	199	HP	0.71951	1.43E-05	0.512008	1.08E-05	-12.3	0.2	10.1	84	9	5	2
B2H3	7.05	7.07	208	HP	0.72023	1.43E-05	0.512054	1.01E-05	-11.4	0.2	10.1	84	10	4	2
B2H3	7.47	7.49	212	HP	0.72457	1.43E-05	0.511991	9.57E-06	-12.6	0.2	10.6	73	18	7	2
B2H4	7.96	7.98	217	HP	0.72105	1.43E-05	0.512031	1.02E-05	-11.8	0.2	10.9	24	57	15	4
B2H5	9.36	9.38	244	HP	0.71537	1.43E-05	0.512099	1.12E-05	-10.5	0.2	11.0	82	11	6	2
B2H5	10.13	10.15	255	HP	0.71804	1.43E-05	0.512091	1.04E-05	-10.7	0.2	9.2	34	44	17	4
A2H2	11.39	11.41	287	HP	0.72108	1.43E-05	0.512065	9.04E-06	-11.2	0.2	8.1	84	9	5	2
A2H3	12.74	12.76	306	HP	0.71909	1.43E-05	0.512123	1.31E-05	-10	0.3	9.5	83	10	5	2
B3H1	13.58	13.6	318	HP	0.72131	1.43E-05	0.512068	7.99E-06	-11.1	0.2	14.2	69	19	9	3
B3H3	15.96	15.98	361	HP	0.7204	1.43E-05	0.512057	9.06E-06	-11.3	0.2	12.7	29	48	20	4
B3H4	17.37	17.39	389	HP	0.72207	1.43E-05	0.512087	1.14E-05	-10.7	0.2	10.2	77	14	7	2
A3H1	19.45	19.47	438	HP	0.72452	1.43E-05	0.512019	8.65E-06	-12.1	0.2	11.5	19	57	20	4
A3H4	22.85	22.87	459	HP	0.71757	1.43E-05	0.512091	1.02E-05	-10.7	0.2	17.2	85	9	4	1
B4H3	25.61	25.63	473	HP	0.7225	1.43E-05	0.512053	1.13E-05	-11.4	0.2	13.7	29	47	20	4
B4H4	27.22	27.24	483	HP	0.71966	1.43E-05	0.512081	1.11E-05	-10.9	0.2	9.3	82	12	5	2
B4H5	29.42	29.44	517	HP	0.71682	1.43E-05	0.512126	1.01E-05	-10	0.2	10.1	84	11	4	2
A4H2	29.4	29.42	525	HP	0.71838	1.43E-05	0.512103	8.75E-06	-10.4	0.2	10.0	78	14	6	2
A4H3	31.98	32	551	HP	0.71791	1.55E-05	0.51215	8.26E-06	-9.5	0.2	10.4	21	55	20	4
A4H4	33.59	33.61	565	HP	0.718	1.46E-05	0.512064	1.08E-05	-11.2	0.2	11.6	77	15	6	2
B5H3	35.85	35.87	583	HP	0.71747	1.43E-05	0.512081	1.22E-05	-10.9	0.2	14.3	84	11	4	1
B5H5	37.6	37.62	599	HP	0.71947	1.43E-05	0.512098	9.41E-06	-10.5	0.2	18.7	32	46	17	5
B2H2	5.93	5.95	177	T	0.72079	1.43E-05	0.511938	9.66E-06	-13.7	0.2	65.0	64	23	10	4
A2H3	11.74	11.76	275	T	0.71971	1.43E-05	0.511974	8.78E-06	-13	0.2	37.1	62	31	6	2
B3H3	17.16	17.18	365	T	0.72091	1.43E-05	0.51197	1.04E-05	-13	0.2	28.0	58	26	13	3